International Journal of Solids and Structures 63 (2015) 184–205

Contents lists available at ScienceDirect

International Journal of Solids and Structures

journal homepage: www.elsevier.com/locate/ijsolstr

Influences of mechanically and dielectrically imperfect interfaces on the reflection and transmission waves between two piezoelectric half spaces

Xiao Guo [a], Peijun Wei [a,b,*], Li Li [a], Qiheng Tang [b]

[a] Department of Applied Mechanics, University of Sciences and Technology Beijing, Beijing 100083, China
[b] State Key Laboratory of Nonlinear Mechanics (LNM), Chinese Academy of Science, Beijing, Beijing 100080, China

ARTICLE INFO

Article history:
Received 8 September 2014
Received in revised form 24 January 2015
Available online 10 March 2015

Keywords:
Imperfect interface
Piezoelectricity
Reflection
Transmission
Energy flux

ABSTRACT

The influences of mechanically and dielectrically imperfect interfaces on the reflection and transmission waves between two piezoelectric half spaces are studied in this paper. First, the secular equations in the traverse isotropic piezoelectric half space are derived from the general dynamic equation. Then, six kinds of imperfect interfaces are considered. These imperfect interfaces include: the mechanically compliant, dielectrically weakly conducting imperfect interface; the mechanically compliant, dielectrically highly conducting imperfect interface; the grounded metallized interface and the low-dielectric interface and their mechanical counterpart, namely, the fixed interface and the slippery interface. These imperfect interface conditions are required to be satisfied by four sets of waves, namely, the quasi-longitudinal wave (QP), the quasi-transverse wave (QSV), the shear horizontal wave (SH) which is decoupled to other waves and the electric-acoustic wave (EA). The algebraic equations resulting from the imperfect interface conditions are solved to obtain the amplitude ratio of various waves and furthermore the reflection and transmission coefficients in terms of the energy flux ratio. The numerical results are obtained for the incident QP wave, the incident QSV wave and the incident SH wave and are validated by the energy conservation principle. The effects of these imperfect interfaces are discussed based on the numerical results. The present study provides useful information for the detection of imperfect interface.

1. Introduction

During the past few decades, the wave propagation in piezoelectric materials has evolved into a significant research due to its unique electromechanical coupling effect. Alshits and Shuvalov (1995) considered a shear horizontal elastic wave inclined incidence on a periodic structure of piezoelectric layers. It was shown that the reflection spectrum exhibited some specific features such as high selectivity, modulation of the heights of the Bragg maximums, and the extinction effect. Jin et al. (2002) studied the Lamb wave propagation in a metallic semi-infinite medium covered with a piezoelectric layer. It was shown that the phase speeds of Lamb wave are asymptotic to the transverse velocity of the piezoelectric layer as the wavenumber increases. Li and Wang (2006) studied disordered and ordered periodic layered piezoelectric composite structures. The phenomenon of wave localization in disordered periodic structures and the properties of frequency passbands and stopbands in ordered periodic structures were observed. Pang et al. (2008) investigated the reflection and refraction of QP and QSV waves incidence obliquely at the interface between piezoelectric and piezomagnetic media. The reflection or transmission waves in the incident plane consist of four kinds of waves. There are the electroacoustic wave (EA) and the magnetic potential wave (MP) in the piezoelectric medium and the magnetoacoustic wave (MA) and the electric potential wave (EP) in the piezomagnetic medium, besides the coupled QP and QSV waves. Rodríguez-Ramos et al. (2011) investigated the behavior of SH wave propagation with oblique incidence in piezocomposite layered systems. The transmission coefficients with respect to the frequency, incidence angle and piezoelectric volume fraction were studied. Singh (2013) studied the reflection and transmission of SH wave at elastic/piezoelectric and piezoelectric/piezoelectric interfaces. The amplitude and energy ratios against the incidence angle were obtained for the Steel/PZT4 and PZT4/PZT-5H interfaces. Lan and Wei (2014) studied the band gaps of laminated piezoelectric phononic crystal with graded interlayer. It was discussed the influences of the graded interlayer with different gradient profiles on the band gap of laminated piezoelectric phononic crystal. Apart from the bulk wave, the surface waves were also studied, for example, Li and Wei (2014) investigated

* Corresponding author at: Department of Applied Mechanics, University of Sciences and Technology Beijing, Beijing 100083, China.
E-mail address: weipj@ustb.edu.cn (P. Wei).

http://dx.doi.org/10.1016/j.ijsolstr.2015.02.050
0020-7683/

the direction dependence of surface wave speed and the influence of electrically and magnetically short/open circuit conditions in the magneto-electro-elastic material. Four kinds of combinations of the short and open circuit conditions were taken into consideration. Because the reflection and transmission of elastic waves at boundary or interface of piezoelectric materials are fundamental for other further researches, it is interesting especially and thus attracted many researchers. Other references related to the reflection and transmission problem also includes Abd-alla and Alsheikh (2009), Abd-alla et al. (2012, 2014) and so on.

In all the aforementioned works, the interface between two different materials was treated as perfect bonded, namely, the displacement, the traction, the electric potential and the normal electric displacement were continuous across interface. In reality, the presence of interfacial defects due to the accumulative interfacial damages and local debonding is unavoidable. Therefore, the influences of imperfect interface with mechanical or dielectrical quantity jump across interface on the wave propagation are interesting. Alshits and Shuvalov (1993) analyzed Bragg resonance and the reflection of a transverse elastic wave from a periodic piezomagnetic structure with thin superconducting interlayers and also from a periodic piezoelectric structure with metallized interfaces. Fan et al. (2006) investigated certain waves which created the fluctuation perpendicular to incident plane and propagated near an imperfectly bonded interface between two half-spaces of different piezoelectric materials. The existence of these waves relies on the imperfection of the interface bonding. Wang and Sudak (2007) studied the influence of mechanically compliant and dielectrically weakly (or highly) conducting interface when presented the analytical solution of a piezoelectric screw dislocation located within one of two joined piezoelectric half-planes. Huang et al. (2009) studied the interfacial SH waves propagating along the imperfectly bonded interface of a magnetoelectric composite consisting of piezoelectric (PE) and piezomagnetic (PM) phases. It was shown that the interfacial imperfection strongly affects the velocity of interfacial shear waves and the interfacial shear waves do not exist for perfect interface. Lan and Wei (2012) studied the dispersive characteristics of elastic waves propagating through laminated piezoelectric phononic crystal with the mechanical imperfect interfaces. It was discussed the influences of the imperfect interface on the dispersive curves and the band gaps of periodic laminated piezoelectric composite. Piliposyan (2012) investigated the problem of the existence and propagation of a surface SH wave at the interface of two magneto-electro-elastic half-spaces. Four sets of boundary conditions, namely, full contact, partial contact with magnetically closed boundaries, partial contact with electrically closed boundaries and no electromagnetic contact, were considered. Pang and Liu (2011) investigated the reflection and transmission of plane waves at an interface between piezoelectric (PE) and piezomagnetic (PM) media. The mechanical imperfection of bonding behavior at the interface was described as the linear spring model. But the dielectrically imperfect interfaces were not considered. Moreover, the energy fluxes of various waves were not calculated and the numerical results were not validated by the energy flux conservation. Besides, the dependence of reflection and transmission coefficients on the apparent wavenumber in the case of imperfect interfaces was ignored too.

In this paper, the influences of six kinds of imperfect interfaces between two piezoelectric half spaces on the energy partition of reflection and transmission waves are firstly considered. Two of them, of most importance, are the mechanically compliant while dielectrically weakly conducting imperfect interface and the mechanically compliant while dielectrically highly conducting imperfect interface. Moreover, the grounded metallized interface and the low-dielectric interface, and their mechanical counterpart, namely, the fixed interface and the slippery interface, are also considered. These imperfect interface conditions result in a set of algebraic equations from them the reflection and transmission coefficients in terms of the displacement amplitude ratio can be obtained and furthermore the reflection and transmission coefficients in terms of the energy flux ratio are calculated. In present work, the reflection and transmission coefficients in terms of the energy flux ratio are provided instead of the displacement amplitude ratio as in most previous literatures because the energy flux ratio can be used directly to validate the numerical results whereas the displacement amplitude ratio cannot. The numerical calculations are performed for three kinds of incident waves, namely, QP wave, QSV wave and SH wave. The effects of these mechanically and dielectrically imperfect interfaces on the energy partition of reflection and transmission waves are discussed based on the numerical results.

2. Secular equation and vibration mode of coupled waves

Two piezoelectric half spaces which are transversely isotropic are imperfectly bonded at plane $x_3 = 0$ and their poling directions are parallel to the x_3 axis, see Fig. 1. The materials at both sides of interface are of different material constants. C_{ijmn}, e_{mij}, ε_{mi} and ρ are the elastic constants, piezoelectric constants, dielectric constants and mass density, respectively. The superscript R and T denote quantities relative to the reflection and transmission waves, respectively.

The constitutive equation of piezoelectric material is (Auld, 1990)

$$\begin{cases} \sigma_{ij} = C_{ijmn}S_{mn} - e_{mij}E_m \\ D_m = e_{mij}S_{ij} + \varepsilon_{mi}E_i \end{cases}, \tag{1}$$

where σ_{ij} and S_{mn} are the stress and strain tensor, respectively. E_m and D_m are the electric field and electric displacement vector, respectively. The strain tensor S_{mn} is related with the displacement vector u_n by

$$S_{mn} = \frac{1}{2}(u_{n,m} + u_{m,n}), \tag{2}$$

and the electric field vector E_m is related with the electric potential φ by

$$E_m = -\varphi_{,m}, \tag{3}$$

in the quasi static electric field approximation.

The mechanical and electrical governing equation can be expressed as

$$\begin{cases} \sigma_{ij,i} = \rho\ddot{u}_j \\ D_{m,m} = 0 \end{cases}. \tag{4}$$

In either plane strain or anti-plane strain case, the displacement field and the electric potential are only the function of x_1 and x_3

$$\begin{cases} \mathbf{u} = \{u_1(x_1, x_3, t), u_2(x_1, x_3, t), u_3(x_1, x_3, t)\} \\ \varphi = \varphi(x_1, x_3, t) \end{cases}, \tag{5}$$

and can be assumed as:

$$\{u_1, u_2, u_3, \varphi\} = \{U_1, U_2, U_3, \Phi\}\exp[i(k_1x_1 + k_3x_3 - \omega t)], \tag{6}$$

where the wavenumber $k = (k_1, k_2, k_3) = (k_1, 0, k_3)$ and k_1 is the apparent wavenumber.

Inserting Eqs. (6) and (1) into Eq. (4) leads to

$$\begin{bmatrix} T_{11} & 0 & T_{13} & T_{14} \\ 0 & T_{22} & 0 & 0 \\ T_{31} & 0 & T_{33} & T_{34} \\ T_{41} & 0 & T_{43} & T_{44} \end{bmatrix} \cdot \begin{Bmatrix} U_1 \\ U_2 \\ U_3 \\ \Phi \end{Bmatrix} = \begin{Bmatrix} 0 \\ 0 \\ 0 \\ 0 \end{Bmatrix}. \tag{7}$$

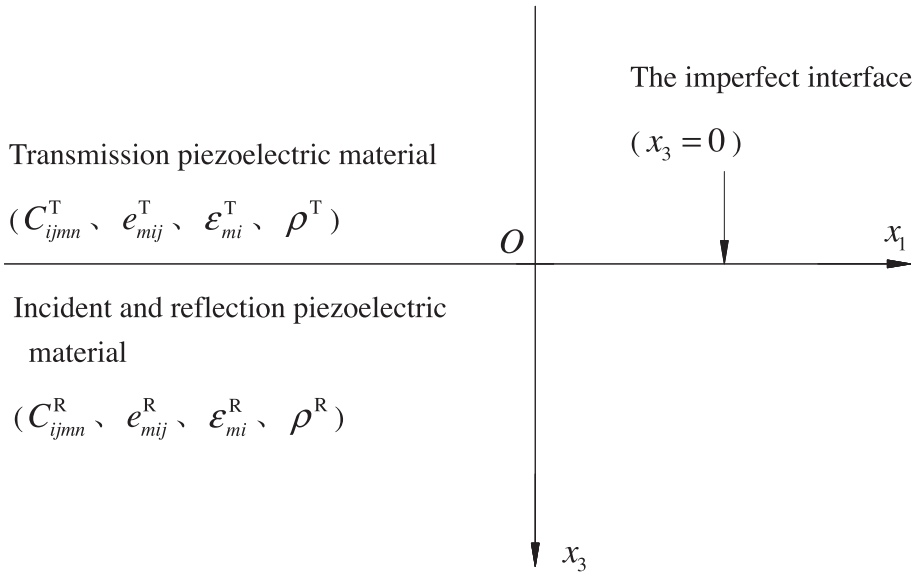

Fig. 1. Two piezoelectric half spaces bonded with an imperfect interface.

The condition of existing non-trivial solution is

$$\begin{vmatrix} T_{11} & T_{13} & T_{14} \\ T_{31} & T_{33} & T_{34} \\ T_{41} & T_{43} & T_{44} \end{vmatrix} = f(\xi, c) = 0. \tag{8a}$$

$$T_{22}(\xi, c) = 0, \tag{8b}$$

where $\xi(=k_3/k_1)$ is the projection ratio of wavenumber vector and $c(=\omega/k_1)$ is the apparent wave speed. The explicit expressions of T_{ij} for the traverse isotropic piezoelectric solid are given in Appendix A.

In this paper, the plane strain related with x_1Ox_3 and the anti-plane strain cases are our main concerns. It is noted from Eq. (8)that the displacement component u_2 is decoupled with the displacement components (u_1, u_3) and the electric potential φ. The incident SH wave only excites the reflection SH wave and the transmission SH wave. However, the incident QP wave or QSV wave can excite the QP wave, the QSV wave and the EA wave as the reflection waves and transmission waves due to the interactive coupling effects among the displacement components u_1, u_3 and the electric potential φ.

In the case of plane strain related with x_1Ox_2 plane and the anti-plane strain, Eq. (6)should be modified as

$$\{u_1, u_2, u_3, \varphi\} = \{U_1, U_2, U_3, \Phi\} \exp[i(k_1x_1 + k_2x_2 - \omega t)], \tag{9}$$

where the wavenumber $k = (k_1, k_2, k_3) = (k_1, k_2, 0)$. As a results of this modification, Eq. (7)becomes

$$\begin{bmatrix} T'_{11} & T'_{12} & 0 & 0 \\ T'_{21} & T'_{22} & 0 & 0 \\ 0 & 0 & T'_{33} & T'_{34} \\ 0 & 0 & T'_{43} & T'_{44} \end{bmatrix} \cdot \begin{Bmatrix} U_1 \\ U_2 \\ U_3 \\ \Phi \end{Bmatrix} = \begin{Bmatrix} 0 \\ 0 \\ 0 \\ 0 \end{Bmatrix}. \tag{10}$$

The explicit expressions of T'_{ij} are also given in Appendix A. In this case, the electric potential φ is coupled with the displacement component u_3 instead of the displacement component u_1 and u_2. The incident SH wave will excite the SH wave and the EA wave as the reflection waves and the transmission waves. The incident QP or QSV wave will excite both QP and QSV waves without EA wave as the reflection waves and the transmission waves.

For a given apparent wave speed c, Eq. (8a)is a polynomial of three orders about ξ^2, and thus there are three pairs of roots about ξ. Similarly, there are one pairs of roots from Eq. (8b). These roots stand for all possible wave modes in the piezoelectric solid. The real roots stand for the bulk waves propagating in the x_1Ox_3 plane. The imaginary roots stand for the evanescent waves which reduce to the surface waves propagating along the interface with the attenuation vertical to the propagation direction. The complex roots stand for the bulk waves accompanied with attenuation. For the traverse isotropic solids considered, the value of ξ indicates that there are eight possible part waves. Six of them are bulk waves and the remnant two part waves are surface waves. Let ξ_1, ξ_3, ξ_5 and ξ_7 are corresponding to the reflection QP wave, the reflection QSV wave, the reflection SH wave and the reflection EA wave, while ξ_2, ξ_4, ξ_6 and ξ_8 the transmission QP wave, the transmission QSV wave, the transmission SH wave and the transmission EA wave. The reflection or transmission angle θ_q can be determined by $\cot\theta_q = \mathrm{Real}(\xi_q)$. It should be noted that all waves except SH wave are the coupled wave with u_1, u_3 and φ keeping a certain coupled relation. Define the amplitude ratio in each coupled wave

$$\begin{cases} G_3 = \frac{U_3}{U_1} = \frac{T_{11}T_{23} - T_{21}T_{13}}{T_{13}T_{24} - T_{14}T_{23}} \\ G_\varphi = \frac{\Phi}{U_1} = \frac{T_{14}T_{21} - T_{11}T_{24}}{T_{13}T_{24} - T_{14}T_{23}} \end{cases}, \tag{11}$$

then, the trio $(1, G_3, G_\varphi)$ stands for the coupled relation in each coupled wave and is called the vibration mode.

3. Imperfect interface and amplitude ratio

When the incident wave is QP wave or QSV wave, the displacement and the electric potential of the incident wave can be expressed as

$$\{u^I_1, u^I_2, u^I_3, \varphi^I\} = \left\{1, 0, G^I_{3q}, G^I_{\varphi q}\right\} U^I_{1q} \exp\left[ik_1\left(x_1 + \xi^I_q x_3 - ct\right)\right], \tag{12}$$

where $q = 2$ denotes incident QP wave and $q = 4$ denotes incident QSV wave. It should be pointed out that the well-known Snell's law, namely, the apparent wavenumbers of various waves are same at the interface, is assumed in Eq. (12). Inserting Eq. (12)into Eq. (1), the traction and the electric displacement related with the incident wave can be expressed as

$$\left\{\sigma_{11}^I,\sigma_{33}^I,\sigma_{31}^I,D_1^I,D_3^I\right\} = ik_1\left\{H_{11q}^I,H_{33q}^I,H_{31q}^I,J_{1q}^I,J_{3q}^I\right\}U_{1q}^I\exp\left[ik_1\left(x_1+\xi_q^I x_3-ct\right)\right]. \quad (13)$$

Similarly,

$$\{u_1^R,u_2^R,u_3^R,\varphi^R\} = \sum_{q=1,3,7}\left\{1,0,G_{3q}^R,G_{\varphi q}^R\right\}U_{1q}^R\exp\left[ik_1\left(x_1+\xi_q^R x_3-ct\right)\right], \quad (14a)$$

$$\left\{\sigma_{11}^R,\sigma_{33}^R,\sigma_{31}^R,D_1^R,D_3^R\right\} = \sum_{q=1,3,7}ik_1\left\{H_{11q}^R,H_{33q}^R,H_{31q}^R,J_{1q}^R,J_{3q}^R\right\}U_{1q}^R\exp\left[ik_1\left(x_1+\xi_q^R x_3-ct\right)\right], \quad (14b)$$

for the reflection waves.

$$\{u_1^T,u_2^T,u_3^T,\varphi^T\} = \sum_{q=2,4,8}\left\{1,0,G_{3q}^T,G_{\varphi q}^T\right\}U_{1q}^T\exp\left[ik_1\left(x_1+\xi_q^T x_3-ct\right)\right], \quad (15a)$$

$$\left\{\sigma_{11}^T,\sigma_{33}^T,\sigma_{31}^T,D_1^T,D_3^T\right\} = \sum_{q=2,4,8}ik_1\left\{H_{11q}^T,H_{33q}^T,H_{31q}^T,J_{1q}^T,J_{3q}^T\right\}U_{1q}^T\exp\left[ik_1\left(x_1+\xi_q^T x_3-ct\right)\right], \quad (15b)$$

for the transmission waves. The explicit expressions of G_{3q}^I, G_{3q}^R, G_{3q}^T, $G_{\varphi q}^I$, $G_{\varphi q}^R$, $G_{\varphi q}^T$, H_{11q}^{I}, H_{11q}^{R}, H_{11q}^{T}, H_{33q}^{I}, H_{33q}^{R}, H_{33q}^{T}, H_{31q}^{I}, H_{31q}^{R}, H_{31q}^{T}, J_{1q}^{I}, J_{1q}^{R}, J_{1q}^{T}, J_{3q}^{I}, J_{3q}^{R}, J_{3q}^{T} are given in Appendix A.

When the incident wave is SH wave, Eqs. (13)–(15)are replaced by

$$\{u_1^I,u_2^I,u_3^I,\varphi^I\} = \{0,1,0,0\}U_{26}^I\exp\left[ik_1(x_1+\xi_6^I x_3-ct)\right], \quad (16a)$$

$$\left\{\sigma_{23}^I,D_2^I\right\} = ik_1\left\{C_{44}^R\xi_6^I,e_{15}^R\xi_6^I\right\}U_{26}^I\exp\left[ik_1(x_1+\xi_6^I x_3-ct)\right], \quad (16b)$$

for the incident SH wave.

$$\{u_1^R,u_2^R,u_3^R,\varphi^R\} = \{0,1,0,0\}U_{25}^R\exp\left[ik_1(x_1+\xi_5^R x_3-ct)\right], \quad (17a)$$

$$\left\{\sigma_{23}^R,D_2^R\right\} = ik_1\left\{C_{44}^R\xi_5^R,e_{15}^R\xi_5^R\right\}U_{25}^R\exp\left[ik_1(x_1+\xi_5^R x_3-ct)\right], \quad (17b)$$

for the reflection SH wave.

$$\{u_1^T,u_2^T,u_3^T,\varphi^T\} = \{0,1,0,0\}U_{26}^T\exp\left[ik_1(x_1+\xi_6^T x_3-ct)\right], \quad (18a)$$

$$\left\{\sigma_{23}^T,D_2^T\right\} = ik_1\left\{C_{44}^T\xi_6^T,e_{15}^T\xi_6^T\right\}U_{26}^T\exp\left[ik_1(x_1+\xi_6^T x_3-ct)\right], \quad (18b)$$

for the transmission SH wave.

For the perfect interface, all mechanical and electrical quantities are continuous across interface. If parts of these mechanical and electrical quantities are not continuous, we call the interface imperfect. Two imperfect interfaces of most importance in reality are the mechanically compliant while dielectrically weakly conducting interface and the mechanically compliant while dielectrically highly conducting interface. For the mechanically compliant interface, tractions are continuous but displacements are discontinuous across the interface and the jump of the displacement components is proportional to their respective interface traction components. For the dielectrically weakly conducting imperfect interface, the normal electric displacement is continuous but the electric potential is discontinuous across the interface and the jump of electric potential is proportional to the normal electric displacement. For the dielectrically highly conducting imperfect interface, the electric potential is continuous but the normal electric displacement is discontinuous across the interface and the jump of the normal electric displacement is proportional to a certain differential expression of the electric potential.

For the mechanically compliant and dielectrically weakly conducting interface, the interface conditions can be expressed as (Wang and Sudak, 2007)

$$\begin{aligned} &u_1^I+u_1^R-u_1^T=\alpha\sigma_{31}^T,\ \ u_2^I+u_2^R-u_2^T=\beta\sigma_{32}^T,\ \ u_3^I+u_3^R-u_3^T=\gamma\sigma_{33}^T\\ &\varphi^I+\varphi^R-\varphi^T=-\eta D_3^T,\ \ D_3^I+D_3^R=D_3^T,\ \ \sigma_{3i}^I+\sigma_{3i}^R=\sigma_{3i}^T.\ \ (i=1,2,3). \end{aligned} \quad (19)$$

For the mechanically compliant and dielectrically highly conducting interface, the interface conditions can be expressed as (Wang and Sudak, 2007)

$$\begin{aligned} &u_1^I+u_1^R-u_1^T=\alpha\sigma_{31}^T,\ \ u_2^I+u_2^R-u_2^T=\beta\sigma_{23}^T,\ \ u_3^I+u_3^R-u_3^T=\gamma\sigma_{33}^T\\ &\varphi^I+\varphi^R=\varphi^T,\ \ D_3^I+D_3^R-D_3^T=\chi\frac{\partial^2\varphi^T}{\partial x_1^2},\ \ \sigma_{3i}^I+\sigma_{3i}^R=\sigma_{3i}^T.\ \ (i=1,2,3). \end{aligned} \quad (20)$$

The parameter α, β and γ in Eqs. (19) and (20) represent the mechanical property of interface and the parameter η and χ the electrical property of interface. The two kinds of imperfect interfaces reduce to the perfect interfaces when these five parameters are all equal to zero. When the mechanical parameters are equal to zero and the electrical parameter η approaches infinity, the mechanically compliant and dielectrically weakly conducting interface reduces to the low-dielectric interface (Alshits and Shuvalov, 1993)

$$\begin{aligned} &u_1^I+u_1^R=u_1^T,\ \ u_2^I+u_2^R=u_2^T,\ \ u_3^I+u_3^R=u_3^T\\ &D_3^I+D_3^R=0,\ \ D_3^T=0,\ \ \sigma_{3i}^I+\sigma_{3i}^R=\sigma_{3i}^T,\ \ (i=1,2,3). \end{aligned} \quad (21a)$$

Another representative interface is the grounded metallized interface (Alshits and Shuvalov, 1993)

$$\begin{aligned} &u_1^I+u_1^R=u_1^T,\ \ u_2^I+u_2^R=u_2^T,\ \ u_3^I+u_3^R=u_3^T\\ &\varphi^I+\varphi^R=0,\ \ \varphi^T=0,\ \ \sigma_{3i}^I+\sigma_{3i}^R=\sigma_{3i}^T,\ \ (i=1,2,3). \end{aligned} \quad (21b)$$

The mechanical parallelism of the grounded metallized interface and the low dielectric interface are the fixed interface

$$u_i^I+u_i^R=u_i^T=0,\ \ (i=1,2,3),\ \ \varphi^I+\varphi^R=\varphi^T,\ \ D_3^I+D_3^R=D_3^T, \quad (22a)$$

and the slippery interface

$$\begin{aligned} &u_3^I+u_3^R=u_3^T,\ \ \sigma_{33}^I+\sigma_{33}^R=\sigma_{33}^T,\ \ \sigma_{3i}^I+\sigma_{3i}^R=\sigma_{3i}^T=0,\ \ (i=1,2)\\ &\varphi^I+\varphi^R=\varphi^T,\ \ D_3^I+D_3^R=D_3^T. \end{aligned} \quad (22b)$$

Physically, the imperfect interface is a result of approximating the thin interlayer (with a finite thickness although very thin) between two dissimilar piezoelectric solids with a mathematic interface without thickness. When the interlayer is rigid and fixed, it leads to the fixed interface; when the interlayer is non-viscous liquid, it leads to slippery interface; when the interlayer is a grounded metal, it leads to the grounded metallized interface; when the interlayer is an insulator, it leads to the low-dielectric interface. The four interfaces are special cases of real interface. Actually, any real interface can be reflected by a set of appropriately selected interface parameter $(\alpha,\beta,\gamma,\eta,\chi)$. The grounded metallized interface and the low-dielectric interface are also called the dielectrically short circuit interface and the open circuit

interface, respectively. Their parallelism, namely, the mechanically short circuit and open circuit interface, are the fixed interface and the slippery interface, respectively.

Inserting Eqs. (12)–(18) into Eqs. (19)–(22)lead to

$$\mathbf{A}\cdot\left(U_{11}^{R},U_{13}^{R},U_{17}^{R},U_{12}^{T},U_{14}^{T},U_{18}^{T}\right)^{T}=\mathbf{a}\cdot U_{1q}^{I}, \tag{23a}$$

for incident QP wave or QSV wave, and

$$\mathbf{B}\cdot\left\{U_{25}^{R},U_{26}^{T}\right\}^{T}=\mathbf{b}\cdot U_{26}^{I}, \tag{23b}$$

for the incident SH wave. The explicit expressions of matrix **A**, **B**, **a** and **b** are given in Appendix B.

4. Energy flux and energy flux conservation

The amplitude ratio of the reflection and the transmission waves relative to the incident wave can be obtained by solving the algebraic equations, Eq. (23a) or (23b). Further, the reflection and transmission coefficients in terms of energy flux ratio can also be obtained. The energy flux density carried by a coupled wave can be expressed as

$$P_i(t)=-\dot{u}_j\sigma_{ji}+\varphi\dot{D}_i, \tag{24}$$

when all physical quantities in Eq. (24) are real valued. The first term indicates the mechanical energy and second term the

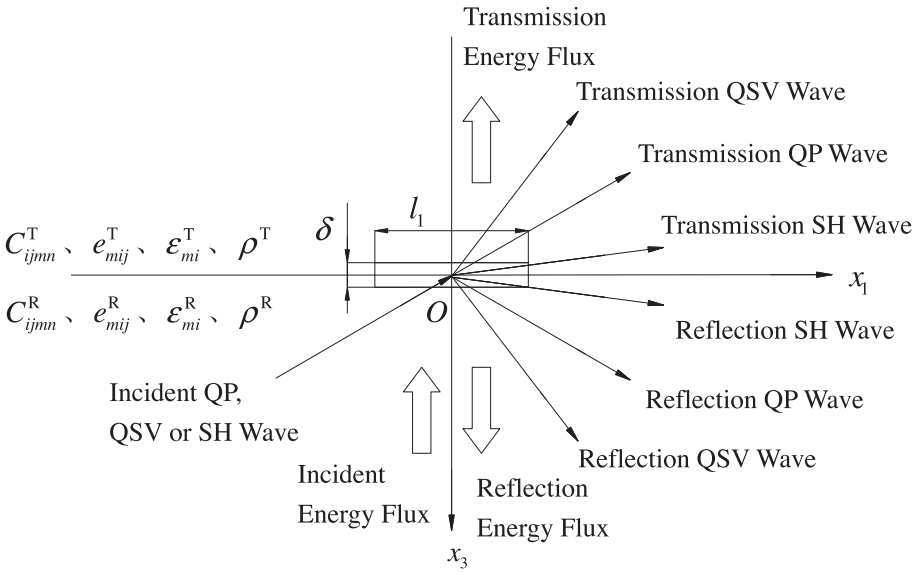

Fig. 2. Sketch of energy flux balance in one thin layer at the interface.

Table 1
Physical constants of ZnO and PZT-4.

	C_{11}	C_{12}	C_{13}	C_{33}	C_{44}	ρ	e_{15}	e_{31}	e_{33}	ε_{11}	ε_{33}
ZnO	20.97	12.11	10.51	21.09	4.247	5680	−0.48	−0.573	1.32	7.570	9.031
PZT-4	13.2	7.1	7.3	11.5	2.6	7500	10.5	−4.1	14.1	710	580

C_{ij} in 10^{10} N · m^{-2}, ρ in kg · m^{-3}, e_{ij} in C · m^{-2}, ε_{ij} in 10^{-11} C^2 · N^{-1} · m^{-2}.

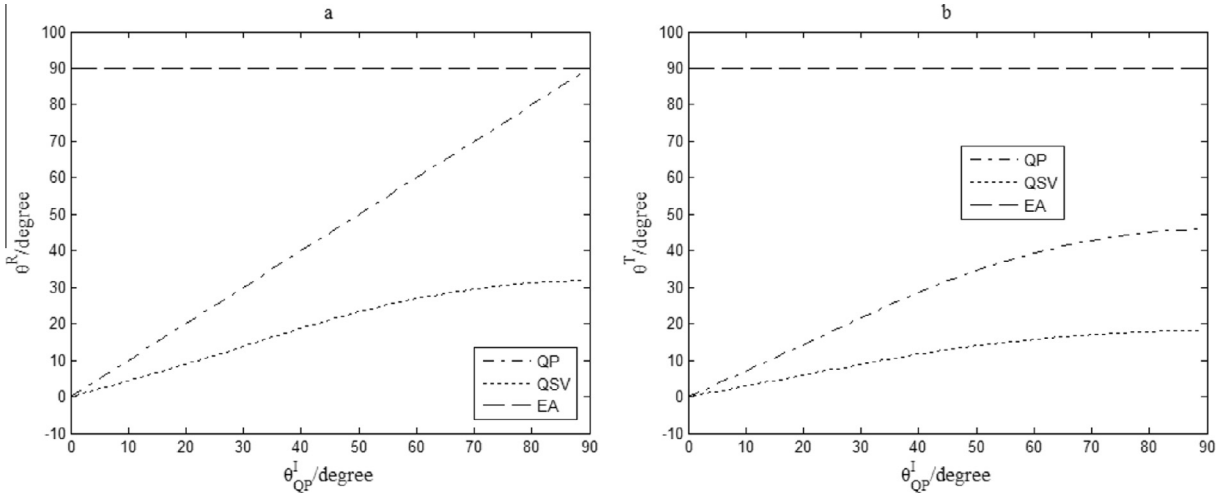

Fig. 3. Reflection and transmission angles in the case of incident QP wave.

electrical energy. Both of them are the periodic function of time and the averaged energy flux in one period is

$$\bar{P}_i = \frac{\omega}{2\pi}\int_{-\pi/\omega}^{\pi/\omega} P_i(t)dt = \frac{1}{2}\mathrm{Re}\left(-\dot{u}_j^*\sigma_{ji} + \varphi\dot{D}_i^*\right), \tag{25}$$

where superscript $*$ in $\dot{u}_i^*$ and $\dot{D}_i^*$ indicates the conjugated complex. Inserting the Eqs. (12)–(18) into Eq. (25), the averaged energy flux along coordinate axis x_1 and x_3 for the incident wave, the reflection wave and the transmission wave can be obtained by

$$\begin{cases} \bar{P}_{1q} = \frac{1}{2}k_1^2 c(H_{11q} + G_{3q}^* H_{31q} + G_{\varphi q} J_{1q}^*)(U_{1q}\cdot U_{1q}^*) \\ \bar{P}_{3q} = \frac{1}{2}k_1^2 c(H_{31q} + G_{3q}^* H_{33q} + G_{\varphi q} J_{3q}^*)(U_{1q}\cdot U_{1q}^*) \end{cases}, \tag{26a}$$

in the case of incident QP or QSV wave, and

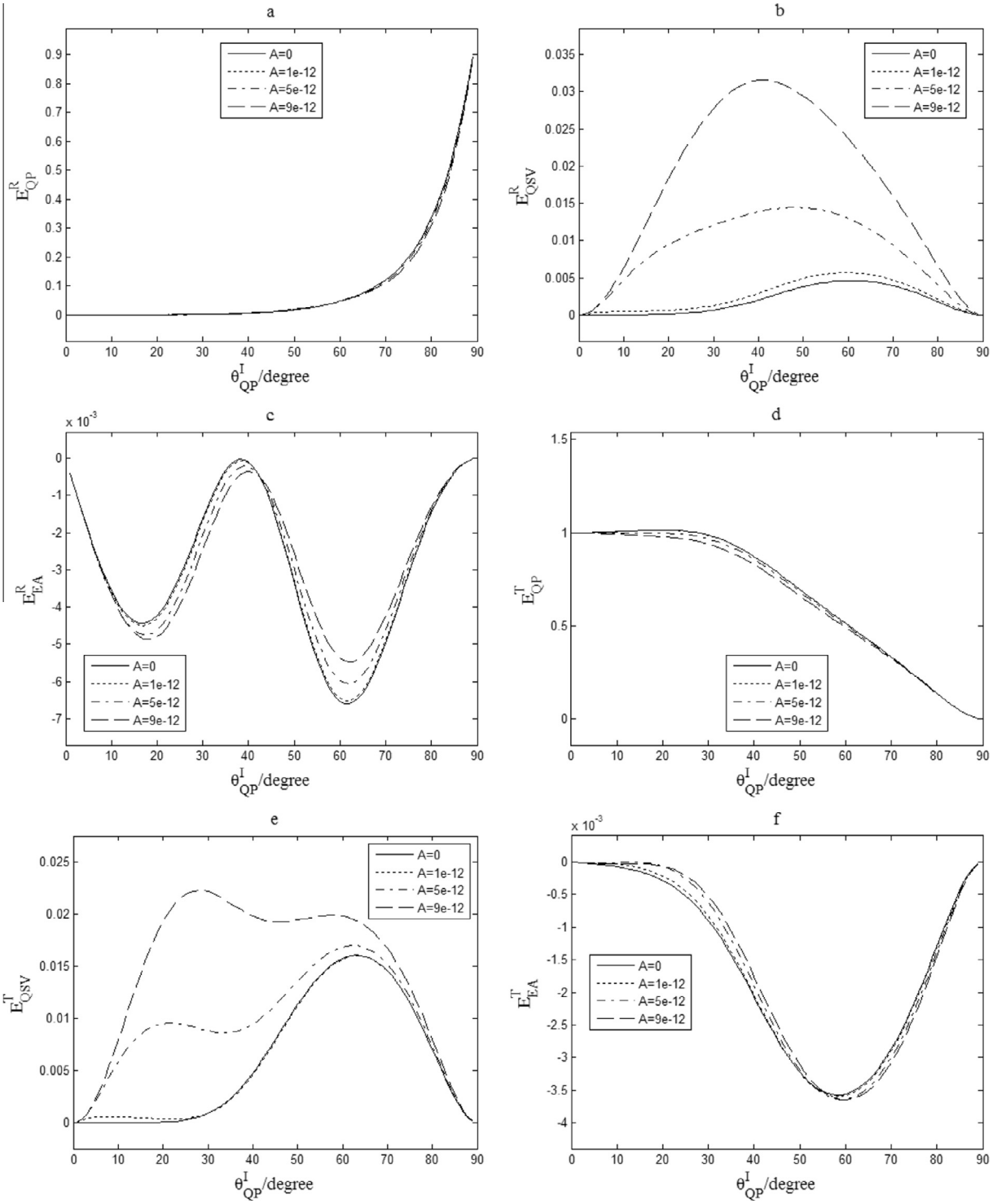

Fig. 4. Effects of the parameter α of the mechanically compliant imperfect interface ($A = \alpha k_1$, $\gamma = 0$, $\eta = 0$ and $\chi = 0$) on the reflection and transmission coefficients in the case of incident QP wave.

$$\begin{cases} \bar{P}_{1q} = \frac{1}{2}k_1^2 cC_{66}(U_{2q} \cdot U_{2q}^*) \\ \bar{P}_{3q} = \frac{1}{2}k_1^2 cC_{44}\xi_q(U_{2q} \cdot U_{2q}^*) \end{cases}, \tag{26b}$$

in the case of incident SH wave. The energy flux along the propagation direction $\boldsymbol{k}_q$ is

$$\bar{P}_q = \bar{P}_{1q}\cos(\mathbf{k_q}, \mathbf{x_1}) + \bar{\mathbf{P}}_{\mathbf{3q}}\cos(\mathbf{k_q}, \mathbf{x_3}). \tag{27}$$

In order to define the energy flux of surface waves, a unit area at the equi-phase surface of surface wave, namely, $x_1 = 0$, with the length of $l_2 \times l_3 = k_1 \times 1/k_1$ is considered. Due to the exponential attenuation of both mechanical and electrical quantities at the equi-phase surface, the energy flux along x_1 axis for the surface wave ($\xi_q = i\bar{\xi}_q$) should be multiplied by a discount factor, i.e. $\int_{-k_1/2}^{k_1/2}\int_0^{1/k_1} e^{-2k_1\bar{\xi}_q x_3}dx_3dx_2 = \frac{1-e^{-2\bar{\xi}_q}}{2\bar{\xi}_q}$ for the reflection surface wave

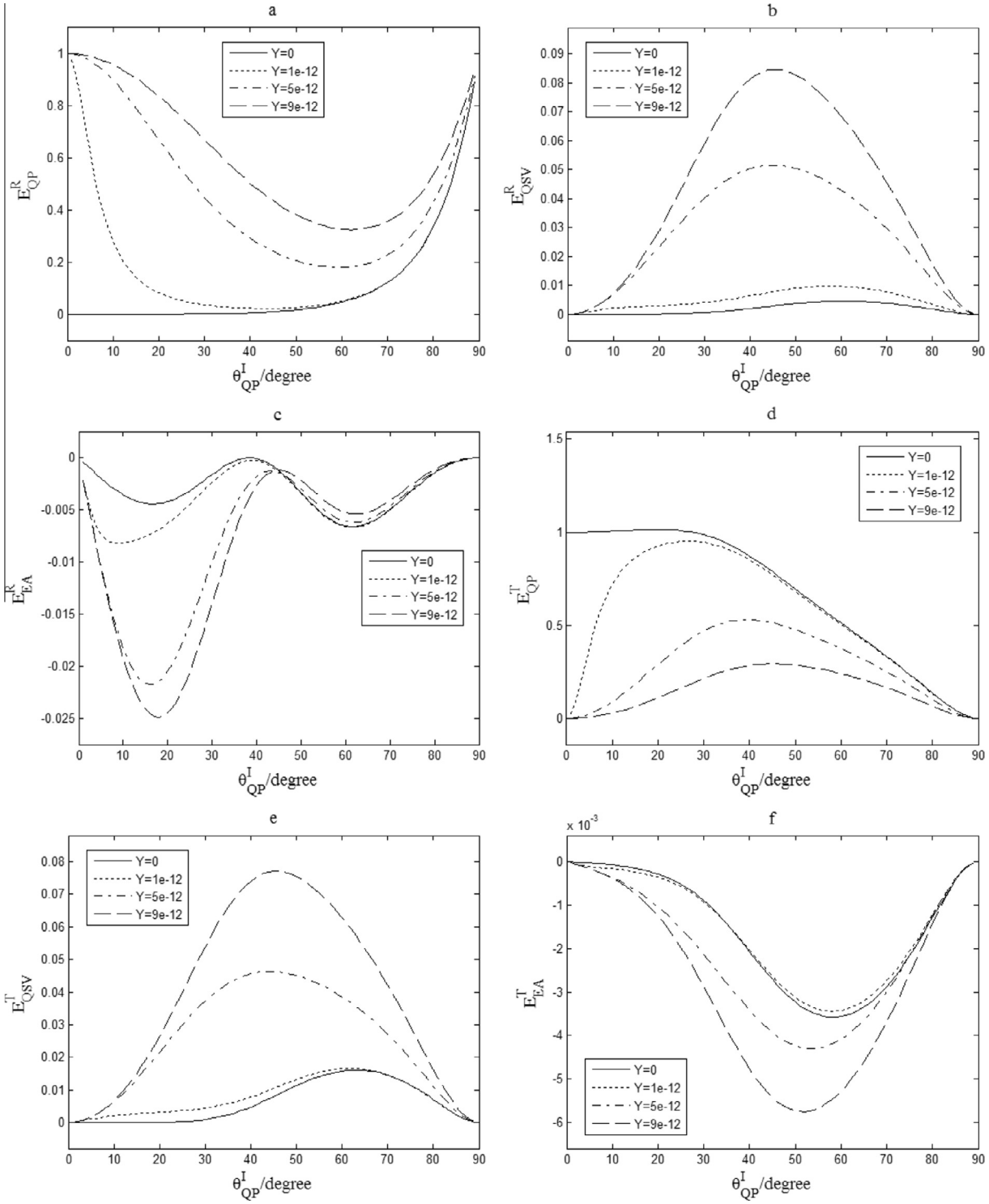

Fig. 5. Effects of the parameter γ of the mechanically compliant imperfect interface ($Y = \gamma k_1$, $\alpha = 0$, $\eta = 0$ and $\chi = 0$) on the reflection and transmission coefficients in the case of incident QP wave.

and $\int_{-k_1/2}^{k_1/2}\int_{-1/k_1}^{0} e^{-2k_1\bar{\xi}_q x_3}dx_3dx_2 = \frac{e^{2\bar{\xi}_q}-1}{2\bar{\xi}_q}$ for the transmission surface wave.

Define the energy reflection and transmission coefficients as the energy flux ratio of the reflection and transmission waves relative to the incident wave, namely,

$$E_s^{R(T)} = \frac{\bar{P}_q}{\bar{P}^I}, \tag{28}$$

where the subscript s indicates QP, QSV, SH and EA wave and the superscript R or T indicates the reflection wave or the transmission wave. In order to validate the numerical results, a thin layer at the interface $x_3 = 0$ with the length of $l_1 \times l_2 = 1/k_1 \times k_1$ and the infinitesimal thickness $\delta \to 0$ is considered, see Fig. 2. The normal energy flux balance requires that the in-put energy flux is equal to the out-put energy flux through the thin layer, namely,

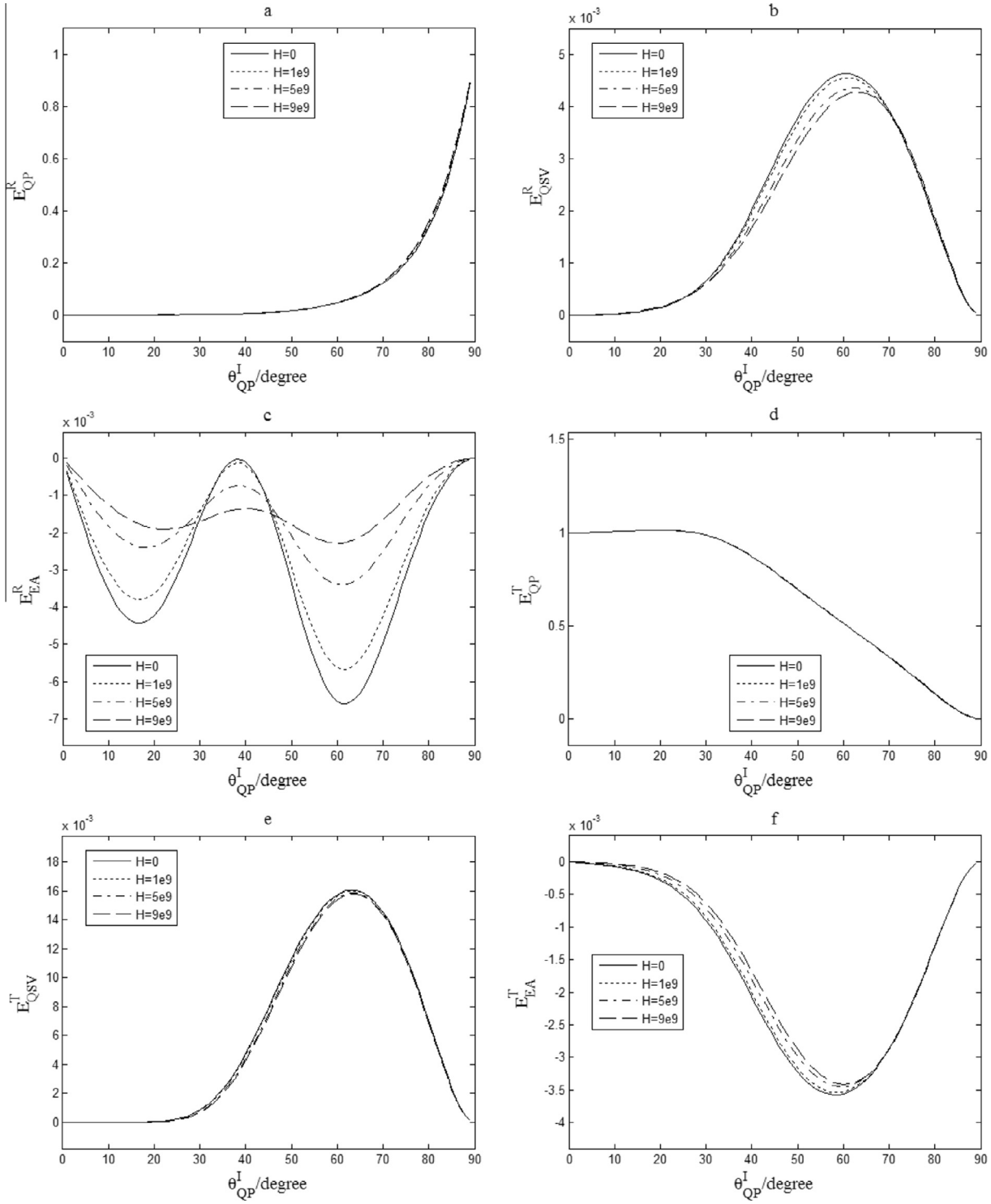

Fig. 6. Effects of the parameter η of the weakly conducting imperfect interface ($H = \eta k_1$, $\alpha = 0$, $\gamma = 0$) on the reflection and transmission coefficients in the case of incident QP wave.

$$E_{bal} = \frac{(\bar{P}_{31} + \bar{P}_{33} + \bar{P}_{37}) + (-\bar{P}_{32} - \bar{P}_{34} - \bar{P}_{38})}{-\bar{P}_3^I} = 1, \tag{29a}$$

in the case of incident QP or QSV wave, and

$$E_{bal} = \frac{\bar{P}_{35} - \bar{P}_{36}}{-\bar{P}_3^I} = 1, \tag{29b}$$

in the case of incident SH wave. Eq. (29) can be used to validate the numerical results.

5. Numerical results and discussion

The material constants of two piezoelectric solids, zinc oxide (ZnO) (Auld, 1990) and ceramics PZT-4 (Jin et al., 2002), are listed in Table 1. The incident wave is assumed to be in the ZnO and propagates obliquely toward to the interface. Three cases, namely, incident QP wave, incident QSV wave and incident SH waves, are considered, respectively. In order to investigate the effects of imperfect interfaces, the energy reflection and transmission

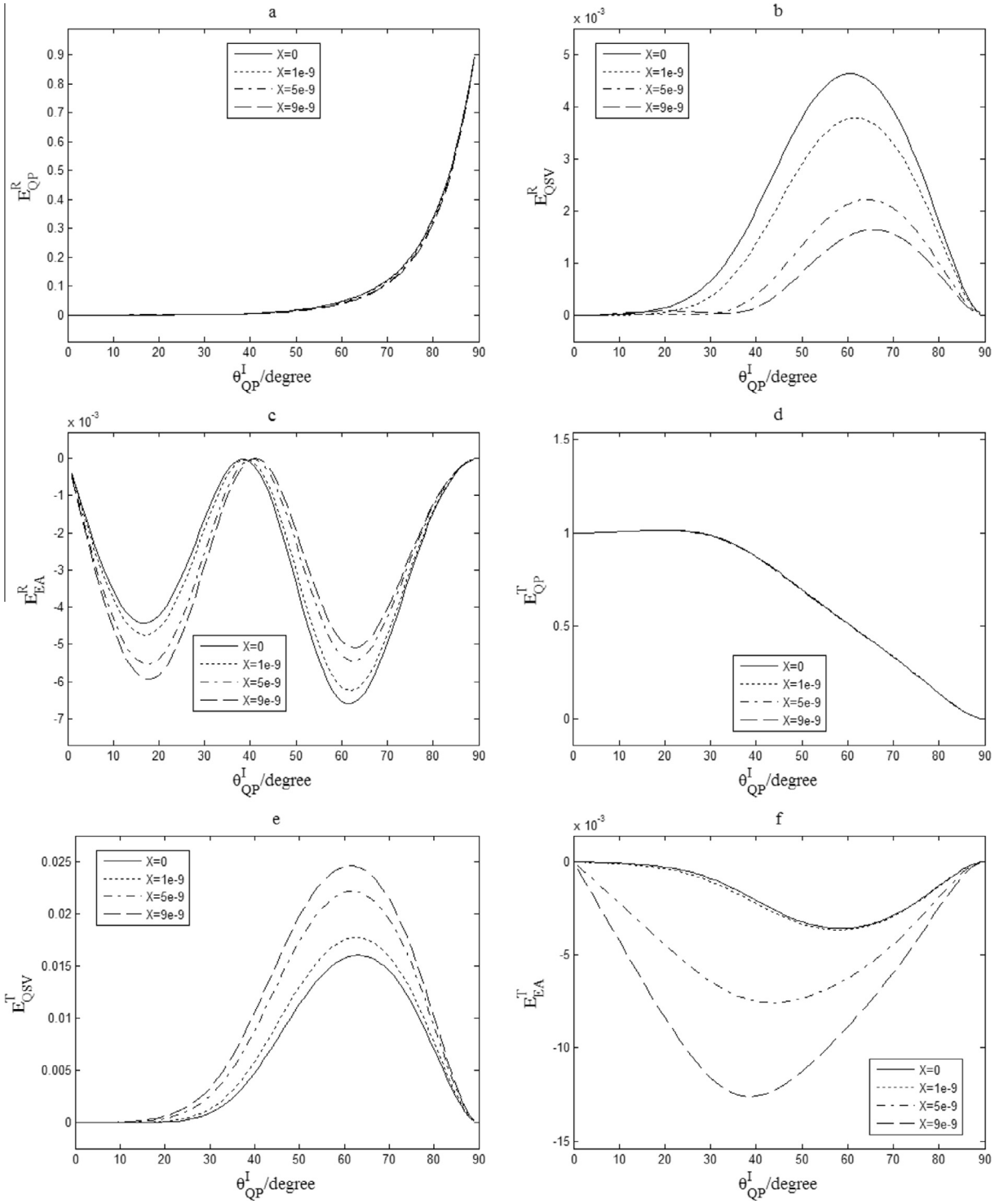

Fig. 7. Effects of the parameter χ of the highly conducting imperfect interface ($X = \chi k_1$, $\alpha = 0$, $\gamma = 0$) on the reflection and transmission coefficients in the case of incident QP wave.

coefficients for the imperfect interface and the perfect interface are both calculated and shown in same figure to facilitate the comparison. In the case of perfect interface, the reflection and transmission coefficients are independent of the apparent wavenumber. However, they are dependent of the apparent wavenumber in the case of the imperfect interface. Therefore, the generalized interface parameters, namely, $A = \alpha k_1$, $B = \beta k_1$, $Y = \gamma k_1$, $H = \eta k_1$ and $X = \chi k_1$ are introduced in the numerical examples. Because the interface parameter α, β and γ are of dimension $N^{-1}\,m^3$, the generalized interface parameters A, B and Y are of dimension $N^{-1}\,m^2$. Similarly, the generalized interface parameters η, χ, H and X are of dimension $N\,m^3\,C^{-2}$, $N^{-1}\,m^{-1}\,C^2$, $N\,m^2\,C^{-2}$ and $N^{-1}\,m^{-2}\,C^2$. The finite value of these interface parameter represents the imperfect degree of interface at the fixed apparent wavenumber.

5.1. In the case of incident QP wave

The reflection and transmission angles in the case of incident QP wave are shown in Fig. 3. It is observed that the reflection angle of QP wave is equal to the incident angle and the reflection angle of

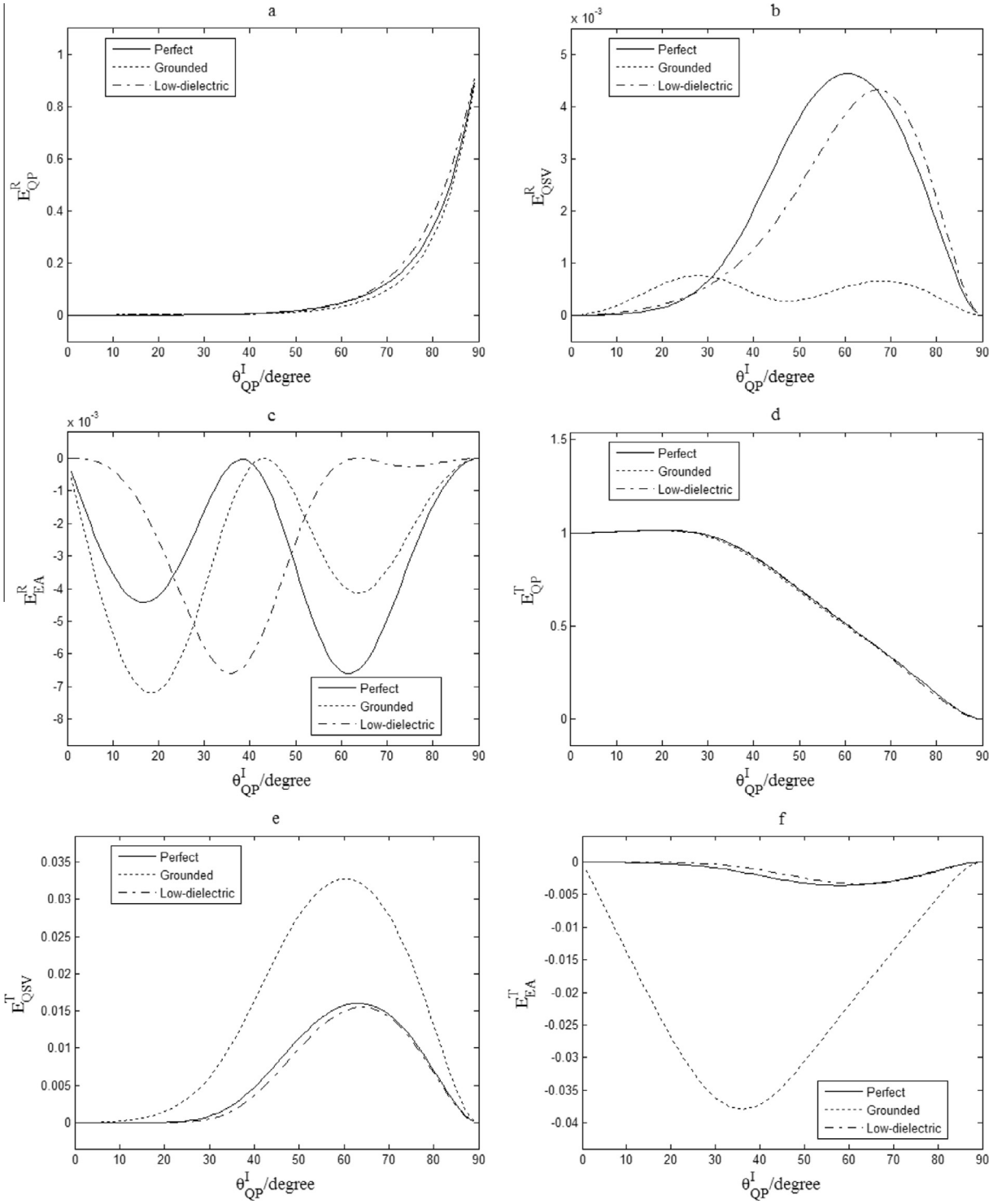

Fig. 8. Effects of the grounded metallized interface and the low-dielectric interface on the reflection and transmission coefficients in the case of incident QP wave.

QSV wave is smaller that of QP wave. The transmission angles are smaller than the reflection angles for same type of wave. EA wave always propagates along interface. No critical angle appears in the case of incident QP wave. It should be pointed out that the imperfect interfaces have no influences on the reflection and transmission angles.

The effects of the interface parameter α and γ of the mechanically compliant imperfect interface on the reflection and transmission coefficients are shown in Figs. 4 and 5. It is observed that the reflection and transmission coefficients of QSV wave increase evidently as the interface parameter α increases. The effects of the interface parameter α on the QP wave are nearly unnoticed and the effects on EA wave are smaller than on QSV wave. Different from the interface parameter α, the interface parameter γ has evident influences on all type of waves. The increasing of interface parameter γ makes the reflection and transmission coefficients of both QSV and EA waves evident increasing but the reflection coefficient increasing while the transmission coefficient decreasing for

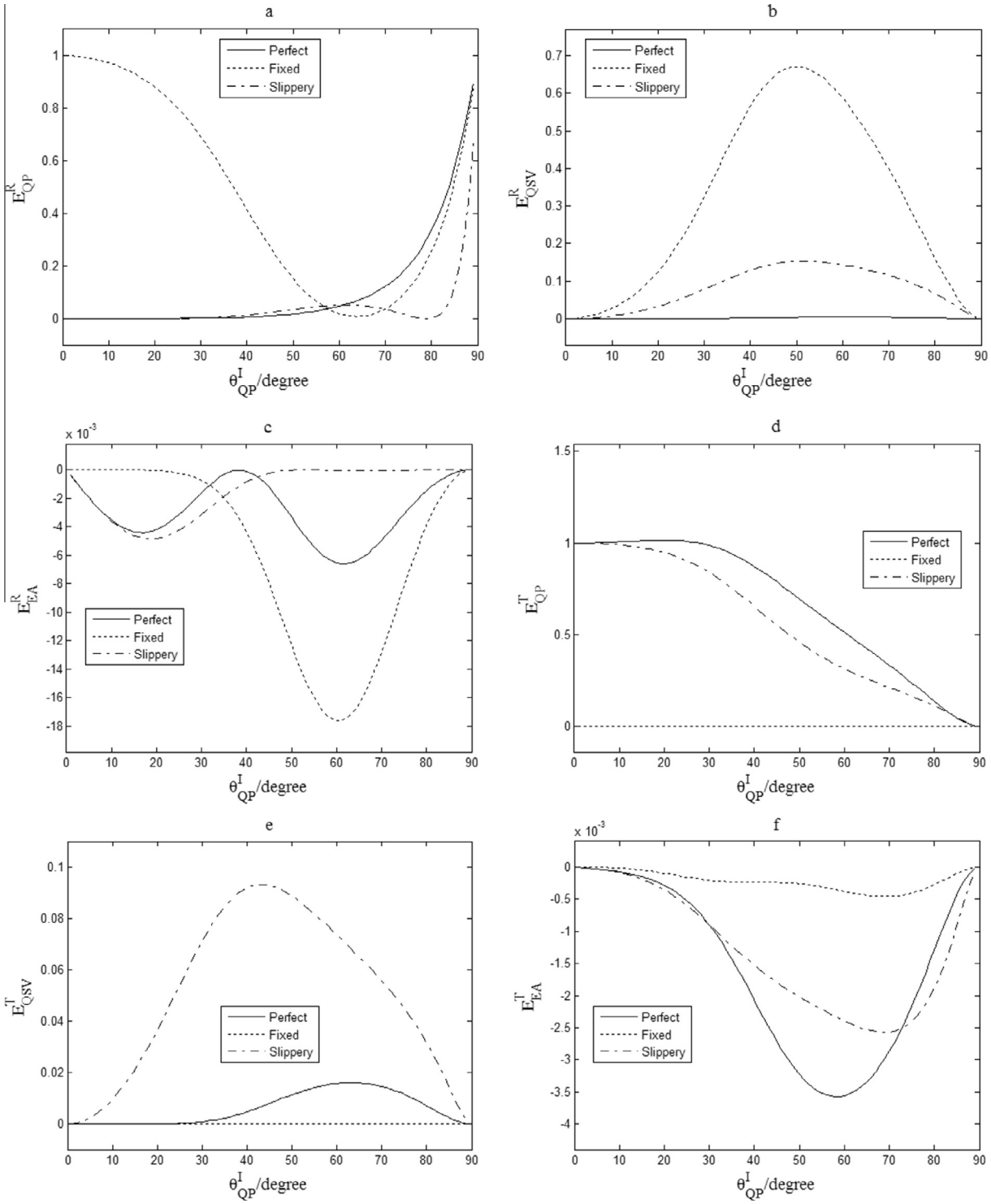

Fig. 9. Effect of the fixed interface and the slippery interface on the reflection and transmission coefficients in the case of incident QP wave.

QP wave. It is noted that the energy flux of EA wave is negative. This is because the electric energy dominates in EA wave and the propagation direction of electrical energy is opposite to the propagation direction of EA wave. In the following discussion, the reflection or transmission coefficient of EA wave means its absolute value without misunderstanding. Compared Figs. 4 and 5, it is found that the mechanically compliant imperfect interface enhances the mode conversion and the normal compliant parameter γ plays more important role than the tangent compliant parameter α .

The effects of the parameter η and the parameter χ on the reflection and transmission coefficients for the weakly conducting and high conducting imperfect interfaces are shown in Figs. 6 and 7. It is observed that the parameter η only has evident influence on EA wave. The increasing of parameter η makes the reflection and transmission of EA wave decreasing and the effects on reflection is more evident than on transmission. However, the parameter χ has evident influences on both of EA and QSV wave. The increasing of parameter of χ makes the transmission of EA and QSV wave evidently increasing while the reflection of QSV evidently decreasing. The reflection coefficient of EA wave may increase or decrease and is dependent of the incident angle. It is interesting that both of interface parameter η and χ have nearly no influences on QP wave. This implies that the dielectrically imperfect interface does not influence QP wave. Compared Figs. 6 and 7, it is found that the interface parameter χ plays more important role than the interface parameter η.

Fig. 8 shows the effects of the grounded metallized interface and the low-dielectric interface. It is observed that the influence of these two kinds of interfaces on QP wave is nearly unnoticeable. The low-dielectric interface has evident influences on the reflection QSV waves and the reflection EA wave while hardly influences on the transmission waves. However, the grounded metallized interface has evident influences on both the reflection QSV and EA waves and the transmission QSV and EA waves and makes the transmission QSV and EA waves evident increasing.

Fig. 9 shows the effects of the fixed interface and the slippery interface. It is observed that the transmission coefficients of all types of waves are close to zero for the fixed interface. This can be explained by that the fixed interface cuts off the propagation of incident wave across interface. Therefore, the energy is focused on the reflection QP wave when the incident angle is close to 0 and 90° and on the reflection QSV wave when the incident angle is near 50°. Compared with the perfect interface, the slippery interface makes the reflection and the transmission coefficients of QSV wave evidently increasing while the reflection and the transmission

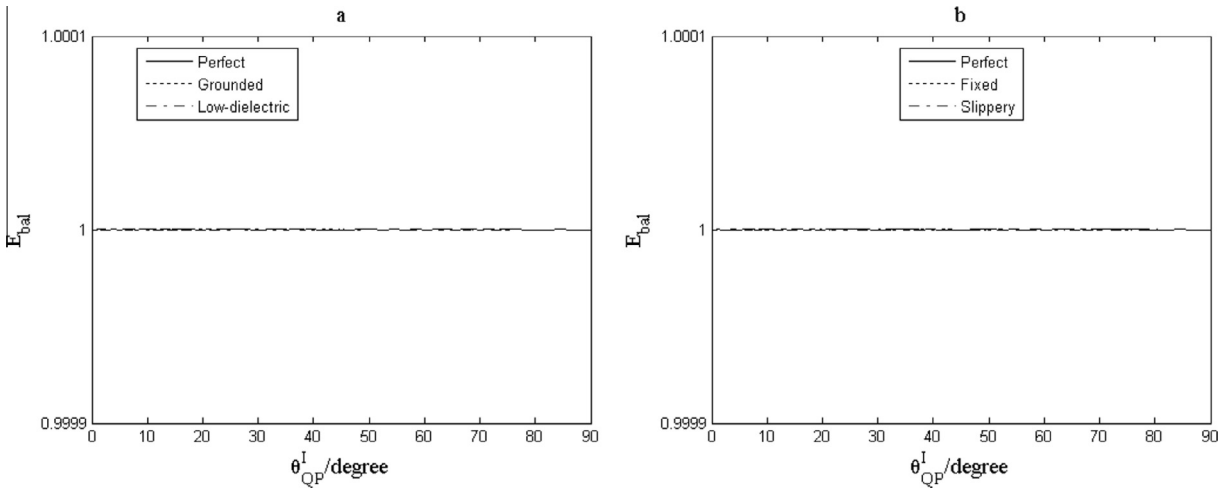

Fig. 10. Balance of normal energy flux for various interface models in the case of incident QP wave.

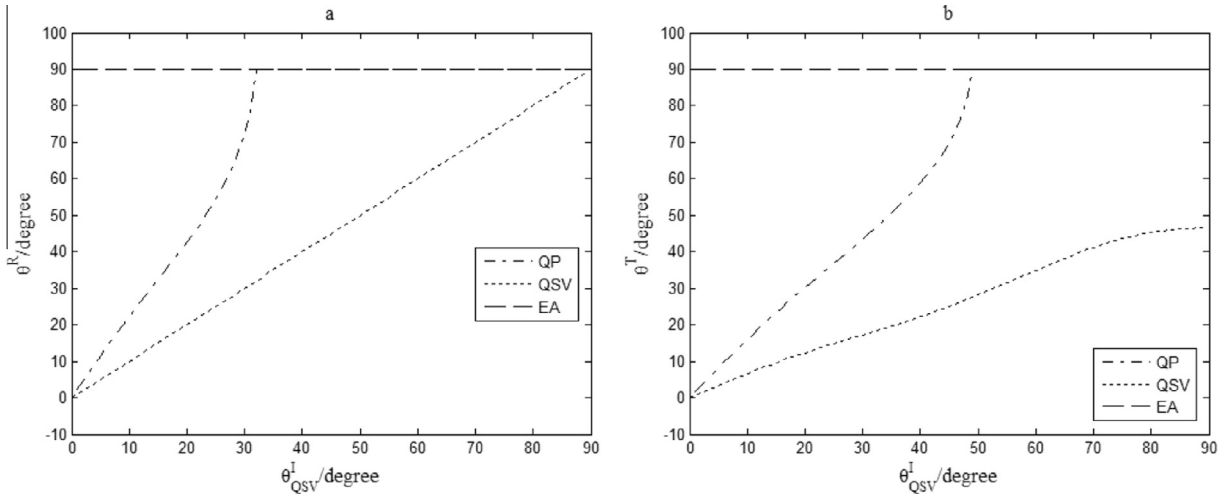

Fig. 11. Reflection and transmission angles in the case of incident QSV wave.

coefficients of QP decreasing. This phenomenon shows that the slippery interface helps to the mode conversation particularly. In fact, the slippery interface is the limit case when the interface parameter $\alpha \to \infty$.

In order to validate the numerical results, the normal energy flux through a thin layer at interface for various interface models are calculated but only the energy flux balances in four cases, namely, the grounded metallized interface, the low-dielectric interface and their mechanical counterpart are shown in Fig. 10. The energy flux balances for imperfect interfaces of the mechanically compliant with dielectrically weakly conducting or dielectrically highly conducting are very similar and are not provided for brevity. It is noticed that the energy flux balance is satisfied exactly for all the interface models mentioned in this paper. This implies

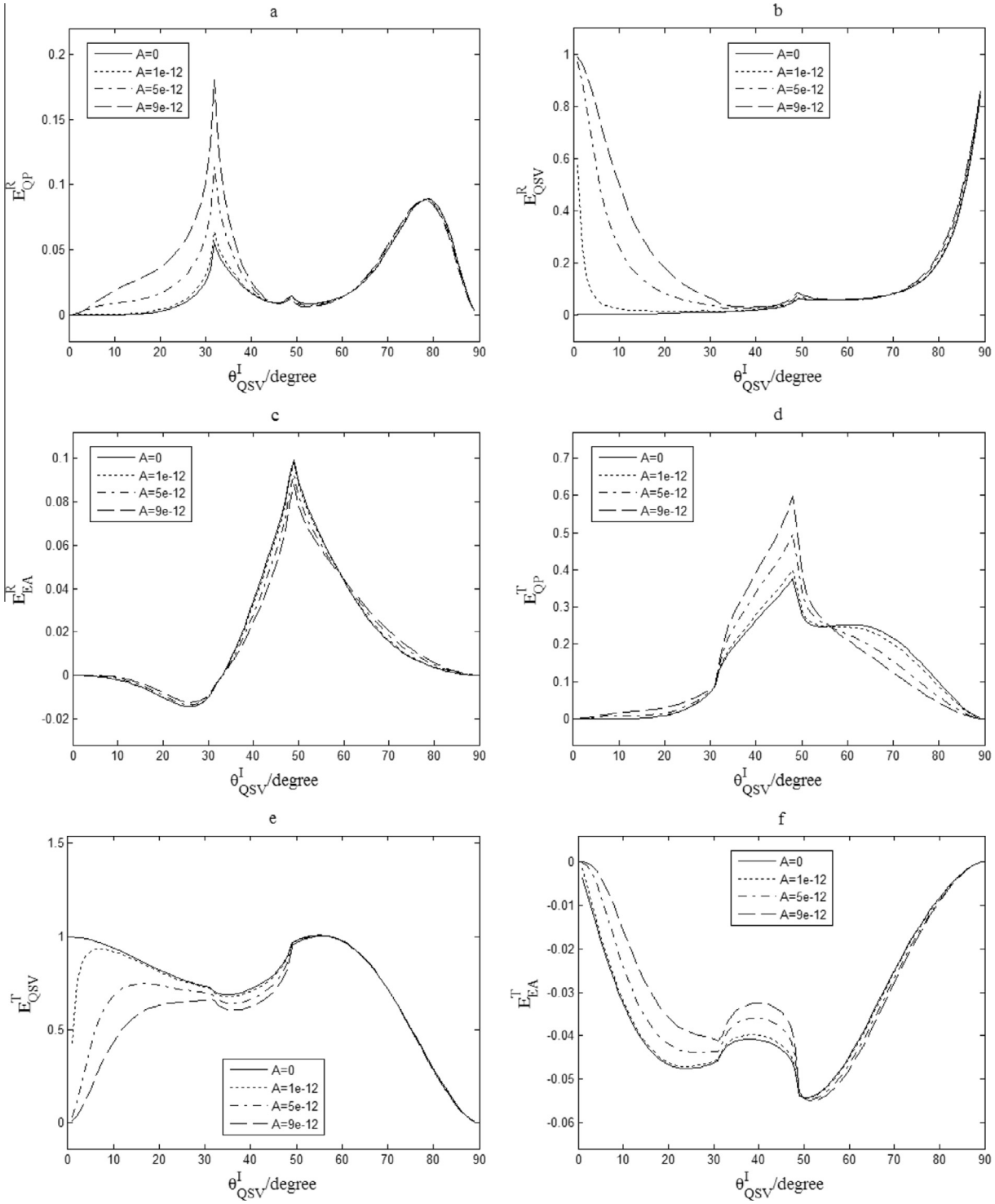

Fig. 12. Effects of the parameter α of the mechanically compliant imperfect interface ($A = \alpha k_1$, $\gamma = 0$, $\eta = 0$ and $\chi = 0$) on the reflection and transmission coefficients in the case of incident QSV wave.

that the imperfect interface may change the energy partition between the reflection wave and the transmission wave but does not create or absorb energy.

5.2. In the case of incident QSV wave

The reflection and transmission angles in the case of incident QSV wave are shown in Fig. 11. It is observed that the reflection angle of QSV wave is always identical with the incident angle. EA wave always propagates along the surface. Different from the incident QP wave, there are two critical angles appearing. One ($\theta_{cr}^1 = 31.8°$) is corresponding with the reflected QP wave reaching 90°; the other ($\theta_{cr}^2 = 48.7°$) is corresponding with the transmission QP wave reaching 90°.

Fig. 12 shows the effects of the interface parameter α on the reflection and transmission coefficients. As in the case of incident QP wave, the effects of the interface parameter α on QSV wave are far greater than on other waves. It is observed that the

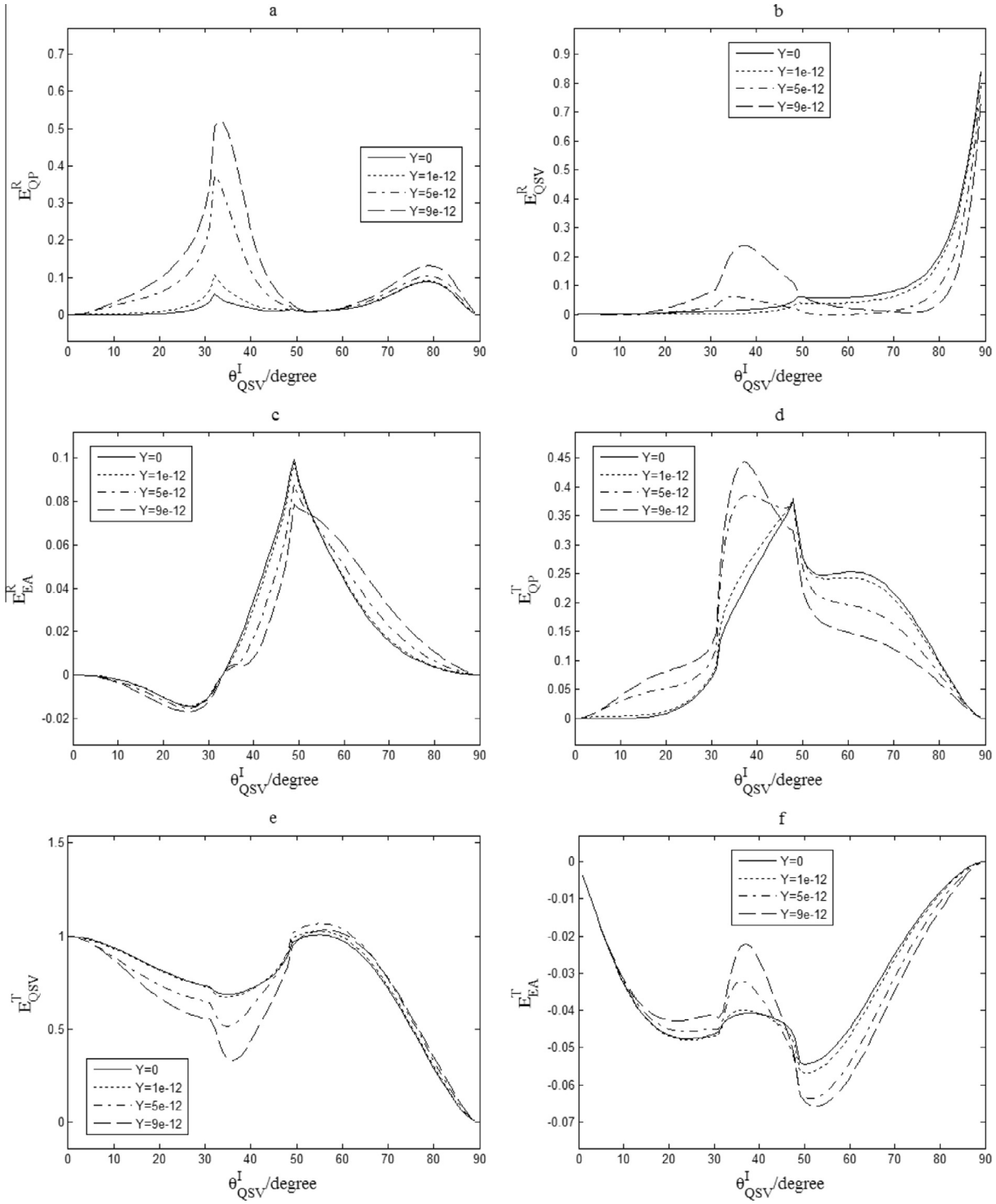

Fig. 13. Effects of the parameter γ of the mechanically compliant imperfect interface ($Y = \gamma k_1$, $\alpha = 0$, $\eta = 0$ and $\chi = 0$) on the reflection and transmission coefficients in the case of incident QSV wave.

increasing of interface parameter α makes the reflection coefficient evident increasing while the transmission coefficient evident decreasing of QSV wave before the second critical angles and has unnoticed influences after the second critical angle. This is different from that in the case of incident QP wave where reflection and transmission of QSV wave both increase as the interface parameter α increases.

Fig. 13 shows the effect of the interface parameter γ on the reflection and transmission coefficients. Different from the interface parameter α, the interface parameter γ has evident influence on all types of waves. In particular, the increasing of the parameter γ makes the reflection QP wave increasing at total range of incident angle. However, the effects of the interface parameter γ on other waves have opposite trends before and after the second critical angle and have opposite trends for the reflection wave and transmission waves. Compared Figs. 12 and 13, it is also observed that the increasing of interface parameter α and γ both enhance the mode conversion.

The effects of electrical parameter η of the weakly conducting imperfect interface on the reflection and transmission coefficients

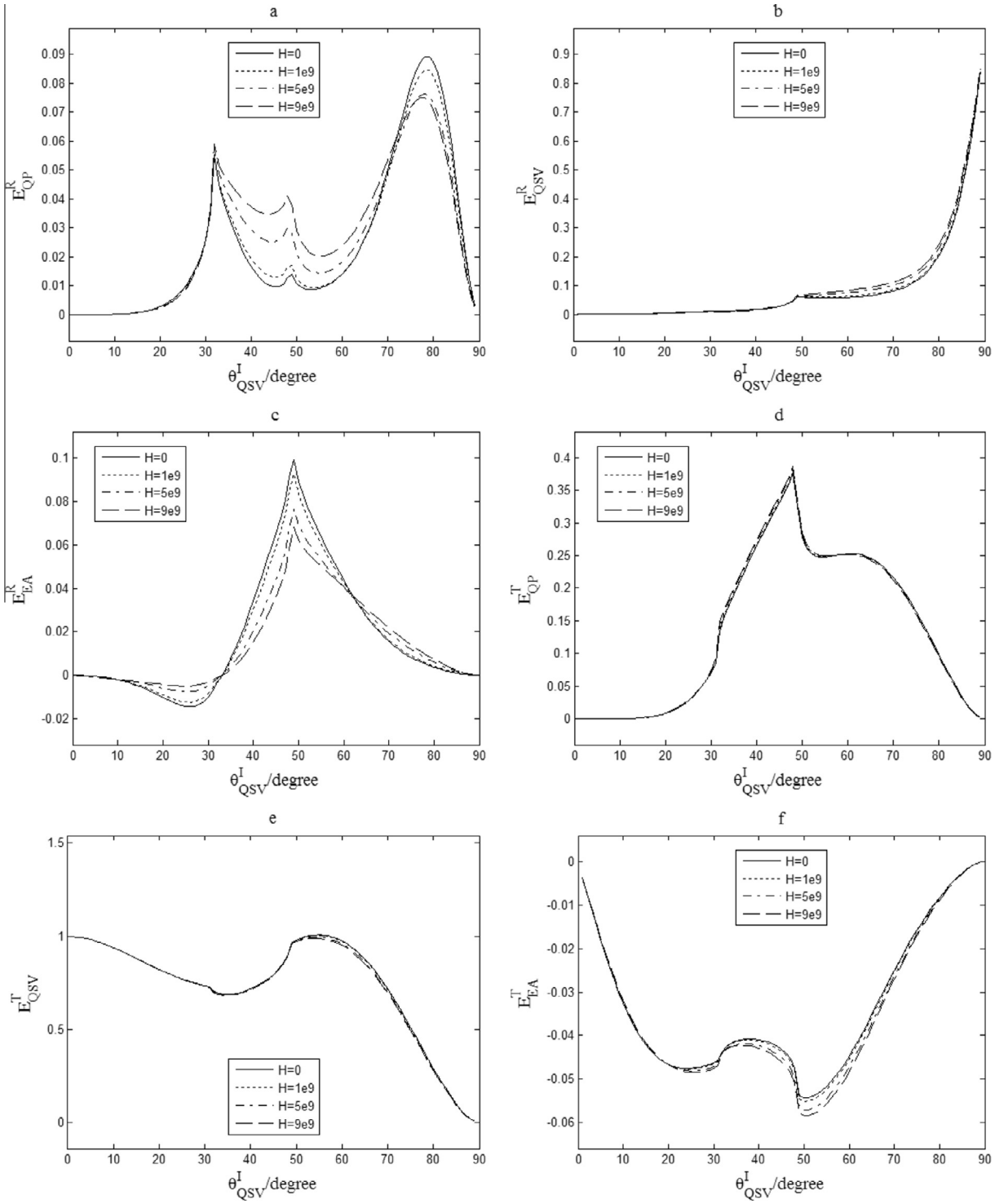

Fig. 14. Effects of the parameter η of the weakly conducting imperfect interface ($H = \eta k_1$, $\alpha = 0$, $\gamma = 0$) on the reflection and transmission coefficients in the case of incident QSV wave.

are shown in Fig. 14. It is observed that the parameter η has only evident influences on the reflection QP wave and slight influence on the reflection EA wave. The influences on the other waves are nearly unnoticed. The effects of the electrical parameter χ of the highly conducting imperfect interface on the reflection and transmission coefficients are shown in Fig. 15. It is observed that the parameter χ has only evident influence on the transmission EA wave and slight influences on all types of reflection waves. The increasing of parameter χ makes the transmission EA wave decreasing and the reflection EA wave increasing at total range of incident angle. However, the reflection QP and QSV waves decrease before the second critical angle and increase after the second critical angle. Moreover, By comparison Figs. 14 and 15, it is also observed that the influences of the two dielectric interface parameters gradually decrease to zero when the incident angle of QSV wave is close to 0° and 90°.

The effects of the grounded metallized interface and the low-dielectric interface on the reflection and transmission coefficients are

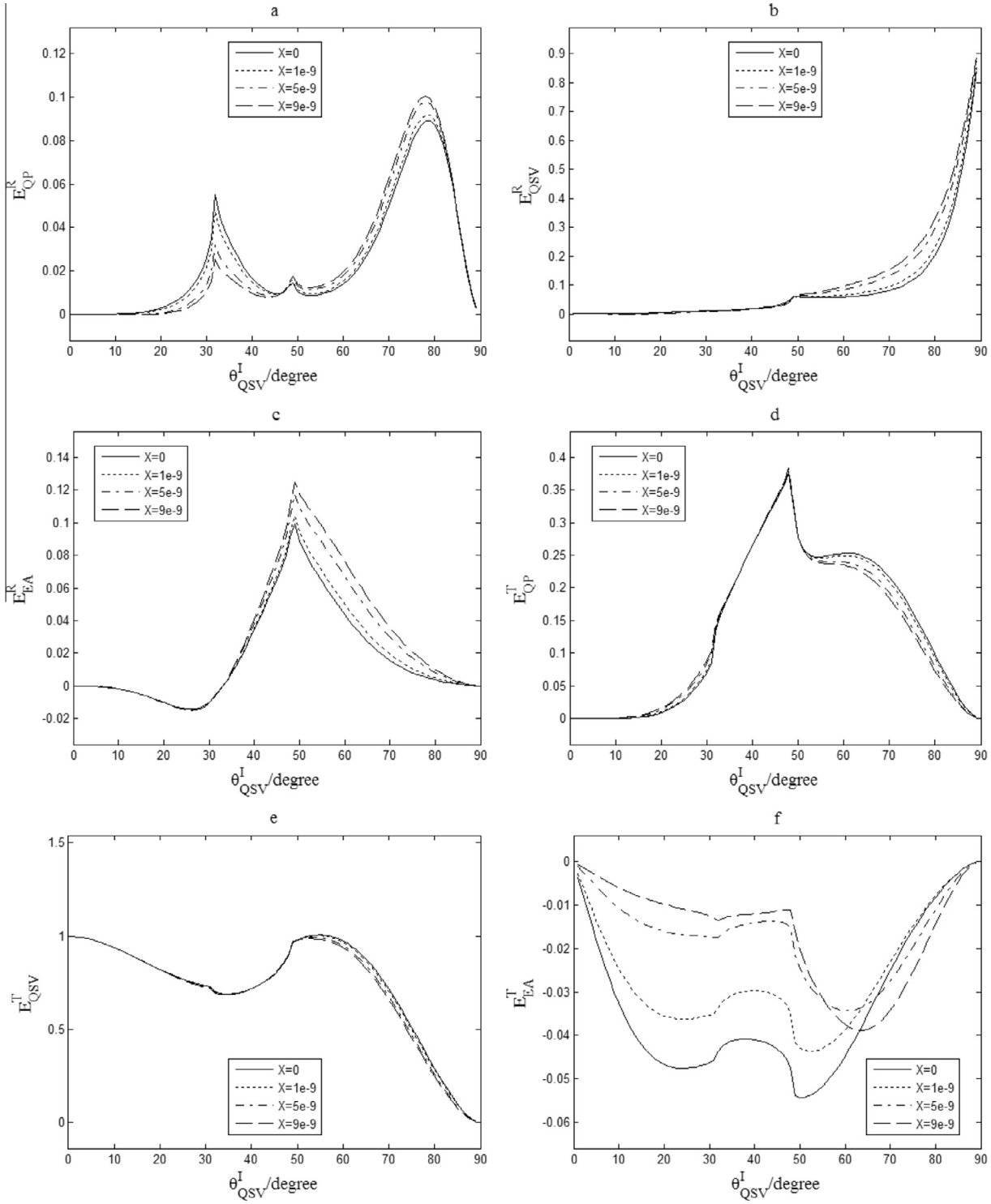

Fig. 15. Effect of the parameter χ of the highly conducting imperfect interface ($X = \chi k_1$, $\alpha = 0$, $\gamma = 0$) on the reflection and transmission coefficients in the case of incident QSV wave.

shown in Fig. 16. It is observed that the low-dielectric interface mainly influence the reflection QP wave and the grounded metallized interface mainly influence EA wave. The low-dielectric interface makes the reflection QP wave evidently increasing but only slight influences on other waves. These observations are completely different from that in the case of incident QP wave.

The reflection and transmission of various waves at the fixed interface and the slippery interface are shown in Fig. 17. As in the case of incident QP, the transmissions of various waves are close to zero because the fixed interface cuts off the propagation of various waves across interface. Near the first critical angle, the reflection QP wave reaches at maximum while the reflection QSV reaches at minimum. The reflection EA wave reaches at minimum near the first critical angle while maximum near the second critical angle. In the case of slippery interface, the transmission coefficients of various waves increase gradually as the incident angle

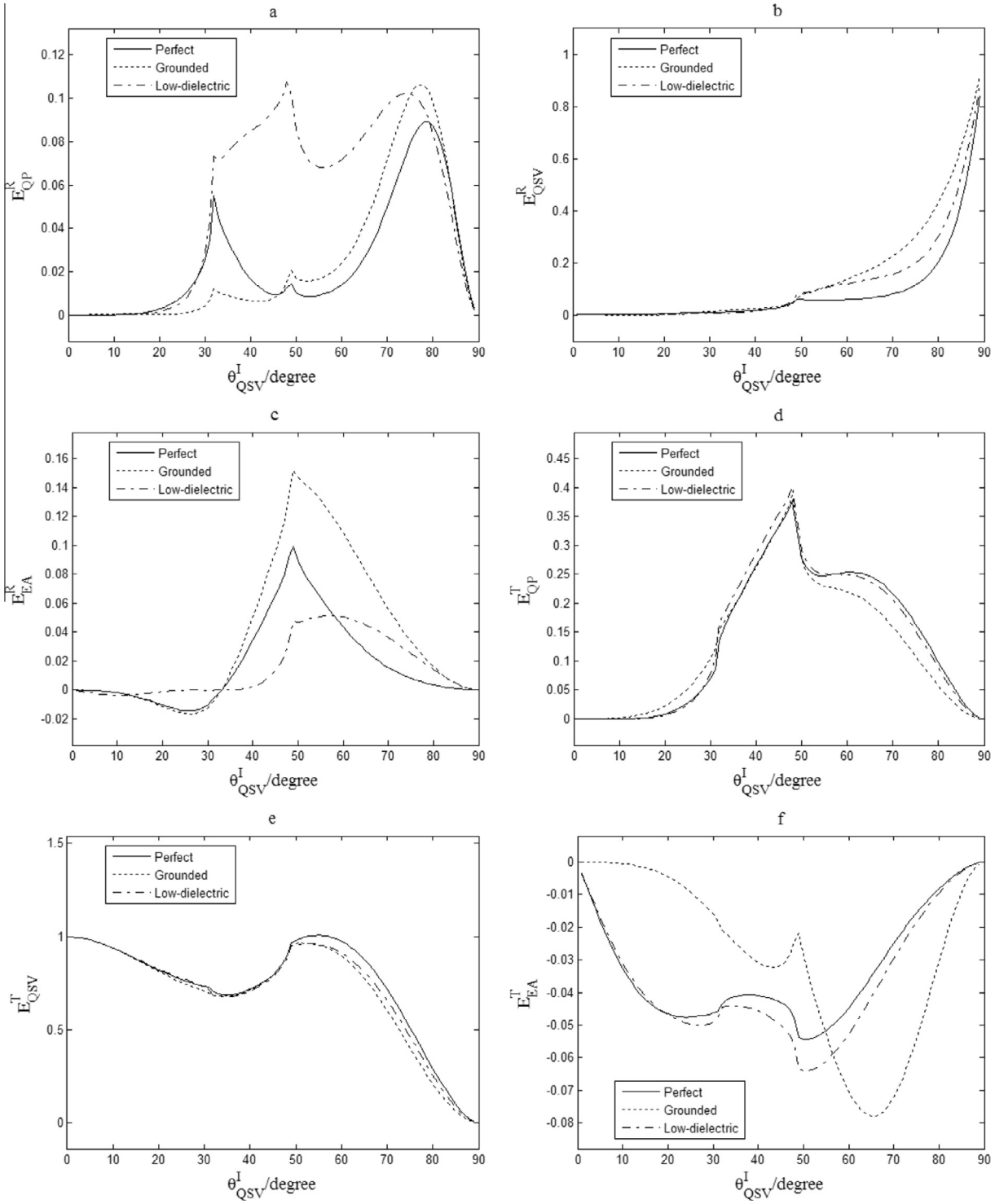

Fig. 16. Effects of the grounded metallized and the low-dielectric interface on the reflection and transmission coefficients in the case of incident QSV wave.

increases and reach at maximum near the second critical angle. The reflection QP wave reaches its maximum near the first critical angle while the reflection QSV wave has two peaks at the first and the second critical angles, respectively.

5.3. In the case of incident SH wave

The reflection and transmission angles in the case of incident SH wave are shown in Fig. 18. Because the mechanical and dielectric fields are decoupled, the dielectrical parameters of the imperfect interfaces don't have any influence on the reflection and transmission coefficients of SH wave. The effects of the parameter β of the compliant imperfect interface on the reflection and transmission coefficients are shown in Fig. 19. It is observed that the parameter β makes the reflection coefficient increasing while the transmission coefficient decreasing. However, the influences gradually decrease to zero as the incident angle increases.

The effects of the fixed interface and the slippery interface on the reflection and transmission coefficients are shown in Fig. 20. Because the anti-plane strain creates only the electric displacement component along x_2 direction, both mechanical energy and the electric energy do not propagate through the fixed and slippery

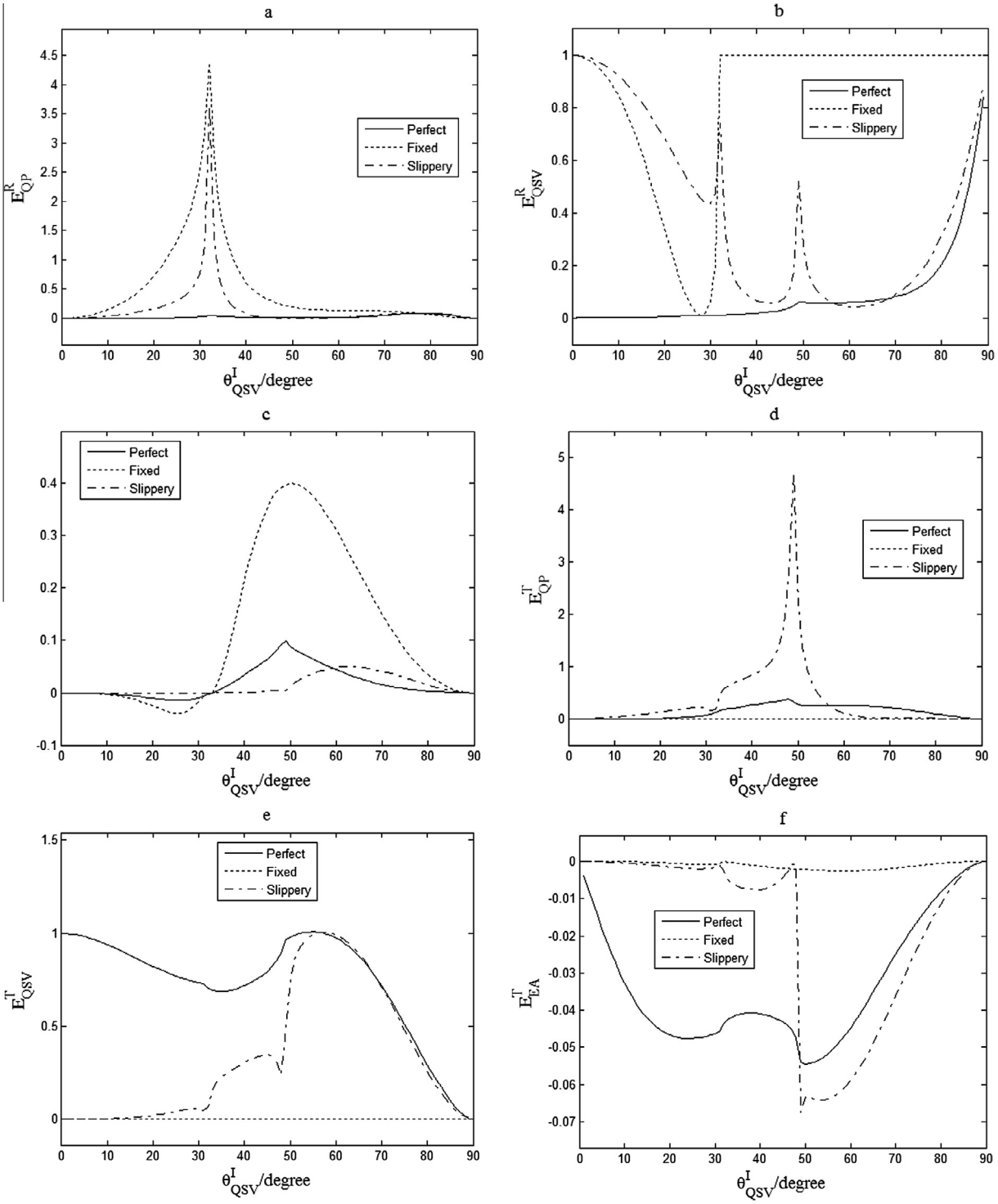

Fig. 17. Effects of the fixed interface and the slippery interface on the reflection and transmission coefficients in the case of incident QSV wave.

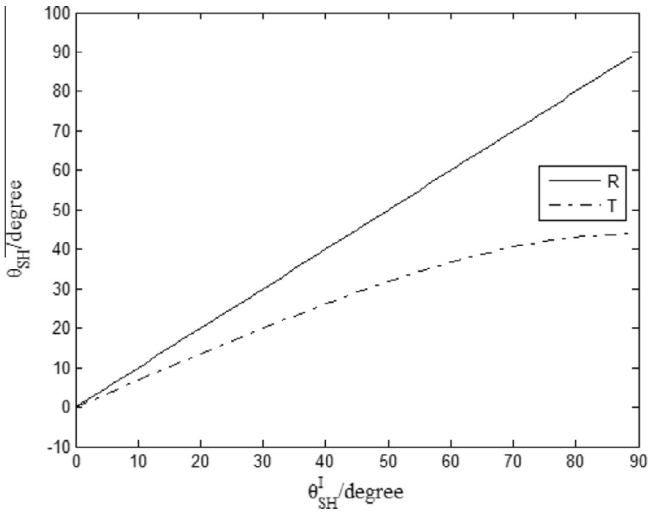

Fig. 18. Reflection and transmission angles in the case of incident SH wave.

interfaces. Thus, the reflection coefficient keeps one and the transmission coefficient keeps zero.

6. Conclusions

Because of the unique coupled behavior between the mechanical field and the electrical field, not only the mechanical energy but also the electric energy can propagate through the interface. The imperfect interface makes the energy propagation and partition at interface more complicated. The systematical study on the imperfect interface can provide us clear physical picture and insight on the energy propagation and partition at the interface. As an example, the material combination ZnO/PZT-4 with various imperfect interfaces is considered and the reflection and transmission coefficients are calculated for incident QP wave, incident QSV wave and incident SH wave, respectively. From the numerical results, the following conclusions can be drawn:

(1) The interface parameter α influences mainly on the QSV wave. the increasing of α makes both reflection and transmission QSV waves increasing in the case of incident QP wave while the reflection QSV wave increasing and the

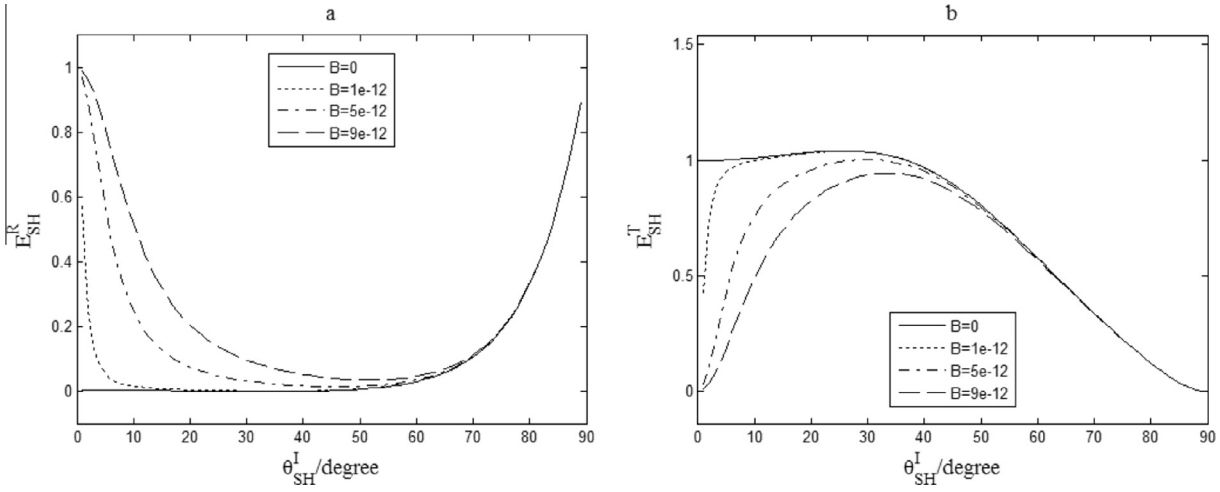

Fig. 19. Effects of the parameter β ($B = \beta k_1$) of the compliant imperfect interface on the reflection and transmission coefficients in the case of incident SH wave.

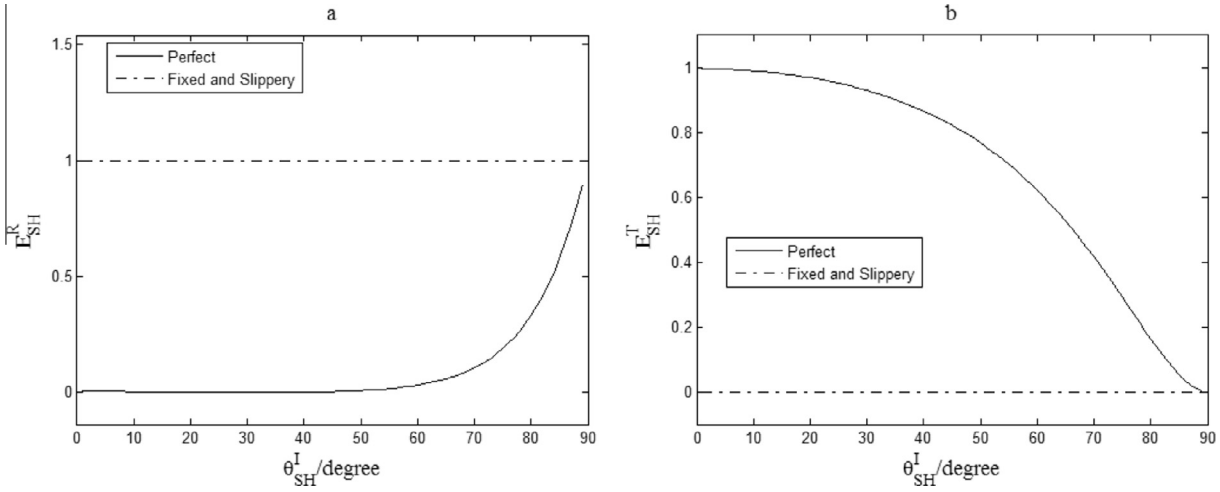

Fig. 20. Effects of the fixed interface and the slippery interface on the reflection and transmission coefficients in the case of incident SH wave.

transmission QSV wave decreasing in the case of incident QSV wave. Obviously, the tangent mechanical imperfect enhances the model conversion at the interface.

(2) The interface parameter γ has influences on all type of waves. In particular, the increasing of interface parameter γ makes both the reflection and transmission QSV waves increasing in the case of incident QP wave while both the reflection and transmission QP wave increasing in the case of incident QSV wave. This means that the normal mechanical imperfect also helps the model conversion at the interface. Moreover, the increasing of interface parameter γ makes the reflection and transmission EA wave increasing under incident QP wave. This means that the normal mechanical imperfect also helps the conversion from mechanical energy to electric energy because the mechanical energy dominates in QP and QSV waves while the electric energy dominates in EA wave.

(3) In the case of incident SH wave, no mode conversion takes place. The increasing of interface parameter β makes the reflection wave increasing and the transmission wave decreasing. The interface parameter η and χ have no influences on the reflection and transmission waves. This means that the mechanical imperfect helps the energy concentration on the reflection wave and the dielectric imperfect has no influence on the energy partition at interface.

(4) Two dielectric interface parameters η and χ have mainly influences on EA wave and QSV wave under incident QP wave while on EA wave and QP wave under incident QSV wave. However, the interface parameters χ plays more important role than the interface parameter η. In contrast with the mechanical imperfect interface parameter, the influences of the dielectric imperfect interface parameter are more dependent upon the incident angle and usually have opposite trend before and after critical angle. Definitely, the influences of the dielectric interface parameter decrease gradually to disappear when the incident angle tends to 0° or 90°.

(5) Compared with the perfect interface, the low-dielectric interface mainly influences the reflection waves and has nearly no influence on the transmission waves. However, the grounded metallized interface has influences on both the reflection waves and the transmission waves. Both the low-dielectric interface and the grounded metallized interface have nearly no influences on QP waves in the case of incident QP wave but have evident influences on the reflection QP wave in the case of incident QSV wave. Moreover, the grounded metallized interface makes the energy of transmission wave evident increasing in the case of incident QP wave but no evident effects on the transmission waves in the case of incident QSV wave.

The mechanically fixed interface can completely cut off the energy propagation through interface and thus makes all transmission waves disappearance no matter of incident QP wave, incident QSV wave and incident SH wave. The mechanically slippery interface can also completely cut off the energy propagation through interface in the case of incident SH wave but cannot in the case of incident QP and QSV waves. The energy carried by the transmission waves is dependent of the incident angle strongly and usually reaches maximum or minimum at critical angles.

Acknowledgements

The work is supported by the National Natural Science Foundation of China (No. 10972029) and Opening Fund of State Key Laboratory of Nonlinear Mechanics (LNM).

Appendix A

For the traverse isotropic piezoelectric solid,

$$\begin{Bmatrix}\sigma_{11}\\ \sigma_{22}\\ \sigma_{33}\\ \sigma_{23}\\ \sigma_{31}\\ \sigma_{12}\end{Bmatrix}=\begin{bmatrix}C_{11}&C_{12}&C_{13}&0&0&0\\ C_{12}&C_{11}&C_{13}&0&0&0\\ C_{13}&C_{13}&C_{33}&0&0&0\\ 0&0&0&C_{44}&0&0\\ 0&0&0&0&C_{44}&0\\ 0&0&0&0&0&C_{66}\end{bmatrix}\cdot\begin{Bmatrix}u_{1,1}\\ u_{2,2}\\ u_{3,3}\\ u_{3,2}+u_{2,3}\\ u_{1,3}+u_{3,1}\\ u_{2,1}+u_{1,2}\end{Bmatrix}-\begin{bmatrix}0&0&e_{31}\\ 0&0&e_{31}\\ 0&0&e_{33}\\ 0&e_{15}&0\\ e_{15}&0&0\\ 0&0&0\end{bmatrix}\cdot\begin{Bmatrix}\varphi_{,1}\\ \varphi_{,2}\\ \varphi_{,3}\end{Bmatrix},$$

$$\begin{Bmatrix}D_1\\ D_2\\ D_3\end{Bmatrix}=\begin{bmatrix}0&0&0&0&e_{15}&0\\ 0&0&0&e_{15}&0&0\\ e_{31}&e_{31}&e_{33}&0&0&0\end{bmatrix}\cdot\begin{Bmatrix}u_{1,1}\\ u_{2,2}\\ u_{3,3}\\ u_{3,2}+u_{2,3}\\ u_{1,3}+u_{3,1}\\ u_{2,1}+u_{1,2}\end{Bmatrix}+\begin{bmatrix}\varepsilon_{11}&0&0\\ 0&\varepsilon_{11}&0\\ 0&0&\varepsilon_{33}\end{bmatrix}\cdot\begin{Bmatrix}\varphi_{,1}\\ \varphi_{,2}\\ \varphi_{,3}\end{Bmatrix},$$

where $C_{66}=0.5(C_{11}-C_{12})$ for Eq. (1). Here, the abbreviative subscript is used instead of the total subscript, and the relation between them please refers to Auld (1990).

$$\begin{aligned}&T_{11}=C_{11}k_1^2+C_{44}k_3^2-\rho\omega^2,\quad T_{22}=C_{66}k_1^2+C_{44}k_3^2-\rho\omega^2,\\ &T_{33}=C_{44}k_1^2+C_{33}k_3^2-\rho\omega^2\\ &T_{44}=-(\varepsilon_{11}k_1^2+\varepsilon_{33}k_3^2),\quad T_{13}=T_{31}=(C_{44}+C_{13})k_3k_1,\\ &T_{14}=T_{41}=(e_{31}+e_{15})k_3k_1\\ &T_{34}=T_{43}=e_{15}k_1^2+e_{33}k_3^2,\quad T_{12}=T_{21}=T_{23}=T_{32}=T_{24}=T_{42}=0\end{aligned}$$

for Eq. (8), and

$$\begin{aligned}&T'_{11}=C_{11}k_1^2+C_{66}k_2^2-\rho\omega^2,\quad T'_{22}=C_{66}k_1^2+C_{11}k_2^2-\rho\omega^2,\\ &T'_{33}=C_{44}k_1^2+C_{44}k_2^2-\rho\omega^2\\ &T'_{44}=-(\varepsilon_{11}k_1^2+\varepsilon_{11}k_2^2),\quad T'_{12}=T'_{21}=(C_{12}+C_{66})k_1k_2,\\ &T'_{34}=T'_{43}=e_{15}k_1^2+e_{15}k_2^2,\\ &T'_{13}=T'_{31}=T'_{14}=T'_{41}=T'_{23}=T'_{32}=T'_{24}=T'_{42}=0\end{aligned}$$

for Eq. (10).

$$G^I_{3q}=\frac{\left(e^R_{31}+e^R_{15}\right)\left(C^R_{44}+C^R_{13}\right)\xi^{I2}_q-\left(C^R_{11}+C^R_{44}\xi^{I2}_q-\rho^Rc^2\right)\left(e^R_{15}+e^R_{33}\xi^{I2}_q\right)}{\left(C^R_{44}+C^R_{13}\right)\left(e^R_{15}+e^R_{33}\xi^{I2}_q\right)\xi^I_q-\left(e^R_{31}+e^R_{15}\right)\left(C^R_{44}+C^R_{33}\xi^{I2}_q-\rho^Rc^2\right)\xi^I_q},$$

$$G^R_{3q}=\frac{\left(e^R_{31}+e^R_{15}\right)\left(C^R_{44}+C^R_{13}\right)\xi^{R2}_q-\left(C^R_{11}+C^R_{44}\xi^{R2}_q-\rho^Rc^2\right)\left(e^R_{15}+e^R_{33}\xi^{R2}_q\right)}{\left(C^R_{44}+C^R_{13}\right)\left(e^R_{15}+e^R_{33}\xi^{R2}_q\right)\xi^R_q-\left(e^R_{31}+e^R_{15}\right)\left(C^R_{44}+C^R_{33}\xi^{R2}_q-\rho^Rc^2\right)\xi^R_q},$$

$$G^T_{3q}=\frac{\left(e^T_{31}+e^T_{15}\right)\left(C^T_{44}+C^T_{13}\right)\xi^{T2}_q-\left(C^T_{11}+C^T_{44}\xi^{T2}_q-\rho^Tc^2\right)\left(e^T_{15}+e^T_{33}\xi^{T2}_q\right)}{\left(C^T_{44}+C^T_{13}\right)\left(e^T_{15}+e^T_{33}\xi^{T2}_q\right)\xi^T_q-\left(e^T_{31}+e^T_{15}\right)\left(C^T_{44}+C^T_{33}\xi^{T2}_q-\rho^Tc^2\right)\xi^T_q},$$

$$G^I_{\varphi q}=\frac{\left(C^R_{11}+C^R_{44}\xi^{I2}_q-\rho^Rc^2\right)\left(C^R_{44}+C^R_{33}\xi^{I2}_q-\rho^Rc^2\right)-\left(C^R_{44}+C^R_{13}\right)^2\xi^{I2}_q}{\left(C^R_{44}+C^R_{13}\right)\left(e^R_{15}+e^R_{33}\xi^{I2}_q\right)\xi^R_q-\left(e^R_{31}+e^R_{15}\right)\left(C^R_{44}+C^R_{33}\xi^{I2}_q-\rho^Rc^2\right)\xi^I_q},$$

$$G^R_{\varphi q}=\frac{\left(C^R_{11}+C^R_{44}\xi^{R2}_q-\rho^R c^2\right)\left(C^R_{44}+C^R_{33}\xi^{R2}_q-\rho^R c^2\right)-\left(C^R_{44}+C^R_{13}\right)^2\xi^{R2}_q}{\left(C^R_{44}+C^R_{13}\right)\left(e^R_{15}+e^R_{33}\xi^{R2}_q\right)\xi^R_q-\left(e^R_{31}+e^R_{15}\right)\left(C^R_{44}+C^R_{33}\xi^{R2}_q-\rho^R c^2\right)\xi^R_q},$$

$$G^T_{\varphi q}=\frac{\left(C^T_{11}+C^T_{44}\xi^{T2}_q-\rho^T c^2\right)\left(C^T_{44}+C^T_{33}\xi^{T2}_q-\rho^T c^2\right)-\left(C^T_{44}+C^T_{13}\right)^2\xi^{T2}_q}{\left(C^T_{44}+C^T_{13}\right)\left(e^T_{15}+e^T_{33}\xi^{T2}_q\right)\xi^R_q-\left(e^T_{31}+e^T_{15}\right)\left(C^T_{44}+C^T_{33}\xi^{T2}_q-\rho^T c^2\right)\xi^T_q},$$

$$J^R_{3q}=e^R_{31}+e^R_{33}G^R_{3q}\xi^R_q-\varepsilon^R_{33}G^R_{\varphi q}\xi^R_q,$$

$$J^T_{3q}=e^T_{31}+e^T_{33}G^T_{3q}\xi^T_q-\varepsilon^T_{33}G^T_{\varphi q}\xi^T_q,$$

for Eqs. (9)–(13).

Appendix B

$$A=\begin{bmatrix}
1 & 1 & 1 & -\left(1-i\alpha k_1H^T_{312}\right) & -\left(1-i\alpha k_1H^T_{314}\right) & -\left(1-i\alpha k_1H^T_{318}\right)\\
G^R_{31} & G^R_{33} & G^R_{37} & -\left(G^T_{32}-i\gamma k_1H^T_{332}\right) & -\left(G^T_{34}-i\gamma k_1H^T_{334}\right) & -\left(G^T_{38}-i\gamma k_1H^T_{338}\right)\\
G^R_{\varphi 1} & G^R_{\varphi 3} & G^R_{\varphi 7} & -\left(G^T_{\varphi 2}+i\eta k_1J^T_{32}\right) & -\left(G^T_{\varphi 4}+i\eta k_1J^T_{34}\right) & -\left(G^T_{\varphi 8}+i\eta k_1J^T_{38}\right)\\
H^R_{331} & H^R_{333} & H^R_{337} & -H^T_{332} & -H^T_{334} & -H^T_{338}\\
H^R_{311} & H^R_{313} & H^R_{317} & -H^T_{312} & -H^T_{314} & -H^T_{318}\\
J^R_{31} & J^R_{33} & J^R_{37} & -J^T_{32} & -J^T_{34} & -J^T_{38}
\end{bmatrix},$$

$$H^I_{11q}=C^R_{11}+C^R_{13}G^I_{3q}\xi^I_q+e^R_{31}G^I_{\varphi q}\xi^I_q,$$

$$H^R_{11q}=C^R_{11}+C^R_{13}G^R_{3q}\xi^R_q+e^R_{31}G^R_{\varphi q}\xi^R_q,$$

$$a=-\left\{1,G^I_{3q},G^I_{\varphi q},H^I_{33q},H^I_{31q},J^I_{3q}\right\}^T,$$

for the mechanically compliant and dielectrically weakly conducting imperfect interface.

$$A=\begin{bmatrix}
1 & 1 & 1 & -\left(1-i\alpha k_1H^T_{312}\right) & -\left(1-i\alpha k_1H^T_{314}\right) & -\left(1-i\alpha k_1H^T_{318}\right)\\
G^R_{31} & G^R_{33} & G^R_{37} & -\left(G^T_{32}-i\gamma k_1H^T_{332}\right) & -\left(G^T_{34}-i\gamma k_1H^T_{334}\right) & -\left(G^T_{38}-i\gamma k_1H^T_{338}\right)\\
G^R_{\varphi 1} & G^R_{\varphi 3} & G^R_{\varphi 7} & -G^T_{\varphi 2} & -G^T_{\varphi 4} & -G^T_{\varphi 8}\\
H^R_{331} & H^R_{333} & H^R_{337} & -H^T_{332} & -H^T_{334} & -H^T_{338}\\
H^R_{311} & H^R_{313} & H^R_{317} & -H^T_{312} & -H^T_{314} & -H^T_{318}\\
J^R_{31} & J^R_{33} & J^R_{37} & -\left(J^T_{32}-i\chi k_1G^T_{\varphi 2}\right) & -\left(J^T_{34}-i\chi k_1G^T_{\varphi 4}\right) & -\left(J^T_{38}-i\chi k_1G^T_{\varphi 8}\right)
\end{bmatrix},$$

$$H^T_{11q}=C^T_{11}+C^T_{13}G^T_{3q}\xi^T_q+e^T_{31}G^T_{\varphi q}\xi^T_q,$$

$$H^I_{33q}=C^R_{13}+C^R_{33}G^I_{3q}\xi^I_q+e^R_{33}G^I_{\varphi q}\xi^I_q,$$

$$H^R_{33q}=C^R_{13}+C^R_{33}G^R_{3q}\xi^R_q+e^R_{33}G^R_{\varphi q}\xi^R_q,$$

$$H^T_{33q}=C^T_{13}+C^T_{33}G^T_{3q}\xi^T_q+e^T_{33}G^T_{\varphi q}\xi^T_q,$$

$$H^I_{31q}=C^R_{44}\left(\xi^I_q+G^I_{3q}\right)+e^R_{15}G^I_{\varphi q},$$

$$H^R_{31q}=C^R_{44}\left(\xi^R_q+G^R_{3q}\right)+e^R_{15}G^R_{\varphi q},$$

$$H^T_{31q}=C^T_{44}\left(\xi^T_q+G^T_{3q}\right)+e^T_{15}G^T_{\varphi q},$$

$$J^I_{1q}=e^R_{15}\left(\xi^I_q+G^I_{3q}\right)-\varepsilon^R_{11}G^I_{\varphi q},$$

$$J^R_{1q}=e^R_{15}\left(\xi^R_q+G^R_{3q}\right)-\varepsilon^R_{11}G^R_{\varphi q},\ J^T_{1q}=e^T_{15}\left(\xi^T_q+G^T_{3q}\right)-\varepsilon^T_{11}G^T_{\varphi q},$$

$$J^I_{3q}=e^R_{31}+e^R_{33}G^I_{3q}\xi^I_q-\varepsilon^R_{33}G^I_{\varphi q}\xi^I_q,$$

$$a=-\left\{1,G^I_{3q},G^I_{\varphi q},H^I_{33q},H^I_{31q},J^I_{3q}\right\}^T,$$

for the mechanically compliant and dielectrically highly conducting imperfect interface.

$$A=\begin{bmatrix}
1 & 1 & 1 & -1 & -1 & -1\\
G^R_{31} & G^R_{33} & G^R_{37} & -G^T_{32} & -G^T_{34} & -G^T_{38}\\
G^R_{\varphi 1} & G^R_{\varphi 3} & G^R_{\varphi 7} & 0 & 0 & 0\\
0 & 0 & 0 & G^T_{\varphi 2} & G^T_{\varphi 4} & G^T_{\varphi 8}\\
H^R_{331} & H^R_{333} & H^R_{337} & -H^T_{332} & -H^T_{334} & -H^T_{338}\\
H^R_{311} & H^R_{313} & H^R_{317} & -H^T_{312} & -H^T_{314} & -H^T_{318}
\end{bmatrix},$$

$$a=-\left\{1,G^I_{3q},G^I_{\varphi q},0,H^I_{33q},H^I_{31q}\right\}^T,$$

for the grounded metallized interface.

$$A=\begin{bmatrix}
1 & 1 & 1 & -1 & -1 & -1\\
G^R_{31} & G^R_{33} & G^R_{37} & -G^T_{32} & -G^T_{34} & -G^T_{38}\\
H^R_{331} & H^R_{333} & H^R_{337} & -H^T_{332} & -H^T_{334} & -H^T_{338}\\
H^R_{311} & H^R_{313} & H^R_{317} & -H^T_{312} & -H^T_{314} & -H^T_{318}\\
J^R_{31} & J^R_{33} & J^R_{37} & 0 & 0 & 0\\
0 & 0 & 0 & J^T_{32} & J^T_{34} & J^T_{36}
\end{bmatrix},$$

$$a = -\left\{1, G^I_{3q}, H^I_{33q}, H^I_{31q}, J^I_{3q}, 0\right\}^T,$$

for the low-dielectric interface.

$$A = \begin{bmatrix} 1 & 1 & 1 & 0 & 0 & 0 \\ 0 & 0 & 0 & 1 & 1 & 1 \\ G^R_{31} & G^R_{33} & G^R_{37} & 0 & 0 & 0 \\ 0 & 0 & 0 & G^T_{32} & G^T_{34} & G^T_{38} \\ G^R_{\varphi 1} & G^R_{\varphi 3} & G^R_{\varphi 7} & -G^T_{\varphi 2} & -G^T_{\varphi 4} & -G^T_{\varphi 8} \\ J^R_{31} & J^R_{33} & J^R_{37} & -J^T_{32} & -J^T_{34} & -J^T_{38} \end{bmatrix},$$

$$a = -\left\{1, 0, G^I_{3q}, 0, G^I_{\varphi q}, J^I_{3q}\right\}^T,$$

for the fixed interface.

$$A = \begin{bmatrix} G^R_{31} & G^R_{33} & G^R_{37} & -G^T_{32} & -G^T_{34} & -G^T_{38} \\ H^R_{331} & H^R_{333} & H^R_{337} & -H^T_{332} & -H^T_{334} & -H^T_{338} \\ H^R_{311} & H^R_{313} & H^R_{317} & 0 & 0 & 0 \\ 0 & 0 & 0 & H^T_{312} & H^T_{314} & H^T_{318} \\ G^R_{\varphi 1} & G^R_{\varphi 3} & G^R_{\varphi 7} & -G^T_{\varphi 2} & -G^T_{\varphi 4} & -G^T_{\varphi 8} \\ J^R_{31} & J^R_{33} & J^R_{37} & -J^T_{32} & -J^T_{34} & -J^T_{38} \end{bmatrix},$$

$$a = -\left\{G^I_{3q}, H^I_{33q}, H^I_{31q}, 0, G^I_{\varphi q}, J^I_{3q}\right\}^T,$$

for the slippery interface.

$$B = \begin{bmatrix} 1 & -\left(1 - i\beta k_1 H^T_{236}\right) \\ H^R_{235} & -H^T_{236} \end{bmatrix}, \quad b = -\left\{1, H^I_{236}\right\}^T,$$

for the mechanically compliant imperfect interface.

$$B = \begin{bmatrix} 1 & 0 \\ 0 & 1 \end{bmatrix}, \quad b = -\{1, 0\}^T,$$

for the fixed interface

$$B = \begin{bmatrix} H^R_{235} & 0 \\ 0 & H^T_{236} \end{bmatrix}, \quad b = -\left\{H^I_{236}, 0\right\}^T,$$

for the slippery interface.

Appendix A. Supplementary data

Supplementary data associated with this article can be found, in the online version, at http://dx.doi.org/10.1016/j.ijsolstr.2015.02.050.

References

Abd-alla, A.N., Alsheikh, F.A., 2009. Reflection and refraction of plane quasi-longitudinal waves at an interface of two piezoelectric media under initial stresses. Arch. Appl. Mech. 79, 843–857.

Abd-alla, A.N., Alsheikh, F.A., Al-Hossain, A.Y., 2012. The reflection phenomena of quasi-vertical transverse waves in piezoelectric medium under initial stresses. Meccanica 47, 731–744.

Abd-alla, A.N., Hamdan, A.M., Giorgio, I., Del Vescovo, D., 2014. The mathematical model of reflection and refraction of longitudinal waves in thermo-piezoelectric materials. Arch. Appl. Mech. 84, 1229–1248.

Alshits, V.I., Shuvalov, A.L., 1993. Bragg reflection of sound in a periodic structure of piezoelectric-crystal layers with superconducting or metalized interlayers. J. Exp. Theor. Phys. 103, 1356–1370.

Alshits, V.I., Shuvalov, A.L., 1995. Resonance reflection and transmission of shear elastic waves in multilayered piezoelectric structures. J. Appl. Phys. 77, 2659–2665.

Auld, B.A., 1990. Acoustic Fields and Waves in Solids. Kriger Publishing Company, Malabar.

Hui, Fan., Yang, Jiashi, Xu, Limei, 2006. Piezoelectric waves near an imperfectly bonded interface between two half-spaces. Appl. Phys. Lett. 88, 203509.

Huang, Y., Li, X.F., Lee, K.Y., 2009. Interfacial shear horizontal (SH) wave propagating in a two-phase piezoelectric/piezomagnetic structure with an imperfect interface. Philos. Mag. Lett. 89, 95–103.

Jin, J., Wang, Q., Quek, S.T., 2002. Lamb wave propagation in a metallic semi-infinite medium covered with piezoelectric layer. Int. J. Solids Struct. 39, 2547–2556.

Lan, Man, Wei, Peijun, 2012. Laminated piezoelectric phononic crystal with imperfect interfaces. J. Appl. Phys., 111, pp. 013505-1–013505-9.

Lan, Man, Wei, Peijun, 2014. Band gap of piezoelectric/piezomagnetic phononic crystal with graded interlayer. Acta Mech. 225, 1779–1794.

Li, Feng-Ming, Wang, Yue-Sheng, 2006. Study on localization of plane elastic waves in disordered periodic 2–2 piezoelectric composite structures. J. Sound Vib. 296, 554–566.

Li, Li., Wei, P.J., 2014. The piezoelectric and piezomagnetic effect on the surface wave velocity of magneto-electro-elastic solids. J. Sound Vib. 333, 2312–2326.

Pang, Yu, Liu, Jin-Xi, 2011. Reflection and transmission of plane waves at an imperfectly bonded interface between piezoelectric and piezomagnetic media. Eur. J. Mech. A/Solids 30, 731–740.

Pang, Yu, Wang, Yue-Sheng, Liu, Jin-Xi, Fang, Dai-Ning, 2008. Reflection and refraction of plane waves at the interface between piezoelectric and piezomagnetic media. Int. J. Eng. Sci. 46, 1098–1110.

Piliposyan, D., 2012. Shear surface waves at the interface of two magneto-electro-elastic media. Multidiscip. Model. Mater. Struct. 8, 417–426.

Rodríguez-Ramos, R., Calás, H., Otero, J.A., Guerra, V., Ramos, A., Wang, Y.S., 2011. Shear horizontal wave in multilayered piezoelectric structures: effect of frequency, incidence angle and constructive parameters. Int. J. Solids Struct. 48, 2941–2947.

Singh, Baljeet, 2013. Propagation of shear waves in a piezoelectric medium. Mech. Adv. Mater. Struct. 20, 434–440.

Wang, X., Sudak, L.J., 2007. A piezoelectric screw dislocation interacting with an imperfect piezoelectric biomaterial interface. Int. J. Solids Struct. 44, 3344–3358.